AD-A088 120 UNIVERSITY OF SOUTHERN CALIFORNIA LOS ANGELES DEPT O--ETC F/G 20/11
OPTICAL AND MECHANICAL PROPERTIES OF INFRARED MATERIALS.(U)
JUL 80 S M COPLEY F49620-78-C-0065
UNCLASSIFIED AFOSR-TR-80-0632 NL

1 OF 1
AD
A088120

END
DATE
FILMED
9-80
DTIC

Unclassified

SECURITY CLASSIFICATION OF THIS PAGE (When Data Entered)

AD A088120

REPORT DOCUMENTATION PAGE

READ INSTRUCTIONS
BEFORE COMPLETING FORM

1. REPORT NUMBER (19) (18) AFOSR-TR- 80-0632	2. GOVT ACCESSION NO. AD-A088 120	3. RECIPIENT'S CATALOG NUMBER
4. TITLE (and Subtitle) (6) Optical and Mechanical Properties of Infrared Materials.		5. TYPE OF REPORT & PERIOD COVERED (9) FINAL rept.
(13)		6. PERFORMING ORG. REPORT NUMBER N/A
7. AUTHOR(s) (10) Stephen M. Copley		8. CONTRACT OR GRANT NUMBER(s) (15) F49620-78-C-0065
9. PERFORMING ORGANIZATION NAME AND ADDRESS University of Southern California Department of Materials Science Los Angeles, CA 90007 (16) 2306		10. PROGRAM ELEMENT, PROJECT, TASK AREA & WORK UNIT NUMBERS 61102F, 2306/C1 (17) C1
11. CONTROLLING OFFICE NAME AND ADDRESS Air Force Office of Scientific Research Bldg. 410 Bolling AFB, D.C. 20332		12. REPORT DATE July 1980
		13. NUMBER OF PAGES 64 (12)
14. MONITORING AGENCY NAME & ADDRESS (if different from Controlling Office) (11) Jul 80 LEVEL II		15. SECURITY CLASS. (of this report) Unclassified
		15a. DECLASSIFICATION/DOWNGRADING SCHEDULE

16. DISTRIBUTION STATEMENT (of this Report)

Approved for public release; distribution unlimited.

17. DISTRIBUTION STATEMENT (of the abstract entered in Block 20, if different from Report)

DTIC
SELECTE
AUG 20 1980
S D
C

18. SUPPLEMENTARY NOTES

19. KEY WORDS (Continue on reverse side if necessary and identify by block number)

IR absorption, Knoop hardness, CaF_2, ZnSe, MgO, KCl
defect complexes, optical properties, mechanical properties
doping.

20. ABSTRACT (Continue on reverse side if necessary and identify by block number)

Optical and mechanical properties of various IR transmitting materials were investigated. Of special interest was the possibility of strengthening such materials through the formation of point defect complexes without increasing their IR absorption. A major facility for determining IR absorption was developed. The materials investigated include alkali halides, alkaline earth fluorides, Al-doped ZnSe and doped MgO. It was

DDC FILE COPY

DD FORM 1473 EDITION OF 1 NOV 65 IS OBSOLETE 409 738 Unclassified found that the hardness of ZnSe doped with Al and CaF_2 doped with Gd could be increased through thermal treatment, however, the identity of the point defect complex producing this hardening could not be determined.

AFOSR-TR- 80-0632

1. STATEMENT OF WORK

F49620-78-C-0065

The goal of this research program is an improved understanding of the roles of microstructure and point defect structure in determining the mechanical and optical properties of infrared materials upon which the development of new materials and novel synthesis techniques can be based. The work statement of the program includes the following items:

a. Determine the optical and mechanical properties of pure and doped alkali halide specimens given various isothermal heat treatments and correlate findings with the microstructures and point defect structures;

b. Conduct similar studies utilizing transmission electron microscopy on specimens of pure and doped alkaline earth fluorides;

c. Investigate the optical and mechanical properties of as-irradiated and annealed ion-implanted layers on zinc selenide and correlate findings with microstructure as determined by transmission electron microscopy;

d. Study the feasibility of preparing a variety of pure and doped infrared materials by evaporation driven liquid sintering;

e. Examine the role of point defect structure and microstructure in determining the optical and mechanical properties of pure and doped magnesium oxide specimens.

Approved for public release; distribution unlimited.

2. ACCOMPLISHMENTS

2.1 Optical Absorption Facility (M. Bass)

A major facility for the study of optical absorption has been established. The facility is shown schematically in Fig. 1. In it, conventional spectrophotometry as indicated by the Cary 14 Spectrophotometer is supplemented by laser calorimetry. The laser calorimetry system includes several CW lasers, an HP 9825 Controller/Calculator based data acquisition, processing and display system and an evacuable calorimeter chamber. This system can measure with a 1 W laser beam an absorption as small as one part in 10^5.

The lasers include a CO_2 laser at 10.6 μm, an HF/DF laser at ∿ 2.4 - 3.8 μm, two Nd:YAG lasers (one at 1.06 and one at 1.318 μm), a Kr ion laser and a dye laser covering the range from 0.35 to 1 μm. The HF/DF laser was received late in the first year from RADC and required an extensive overhaul before it could be reliably operated. It was nearly ready for use at the time of termination of this project.

2.2 Two Photon Absorption Studies (M. Bass, E. W. VanStryland and A. F. Stewart)

Early in this program, while preparing the laser calorimetry facility, we conducted experiments concerning two-photon absorption. This work is described in an "Applied Physics Letters" article, which is attached to this report (see Appendix 1).

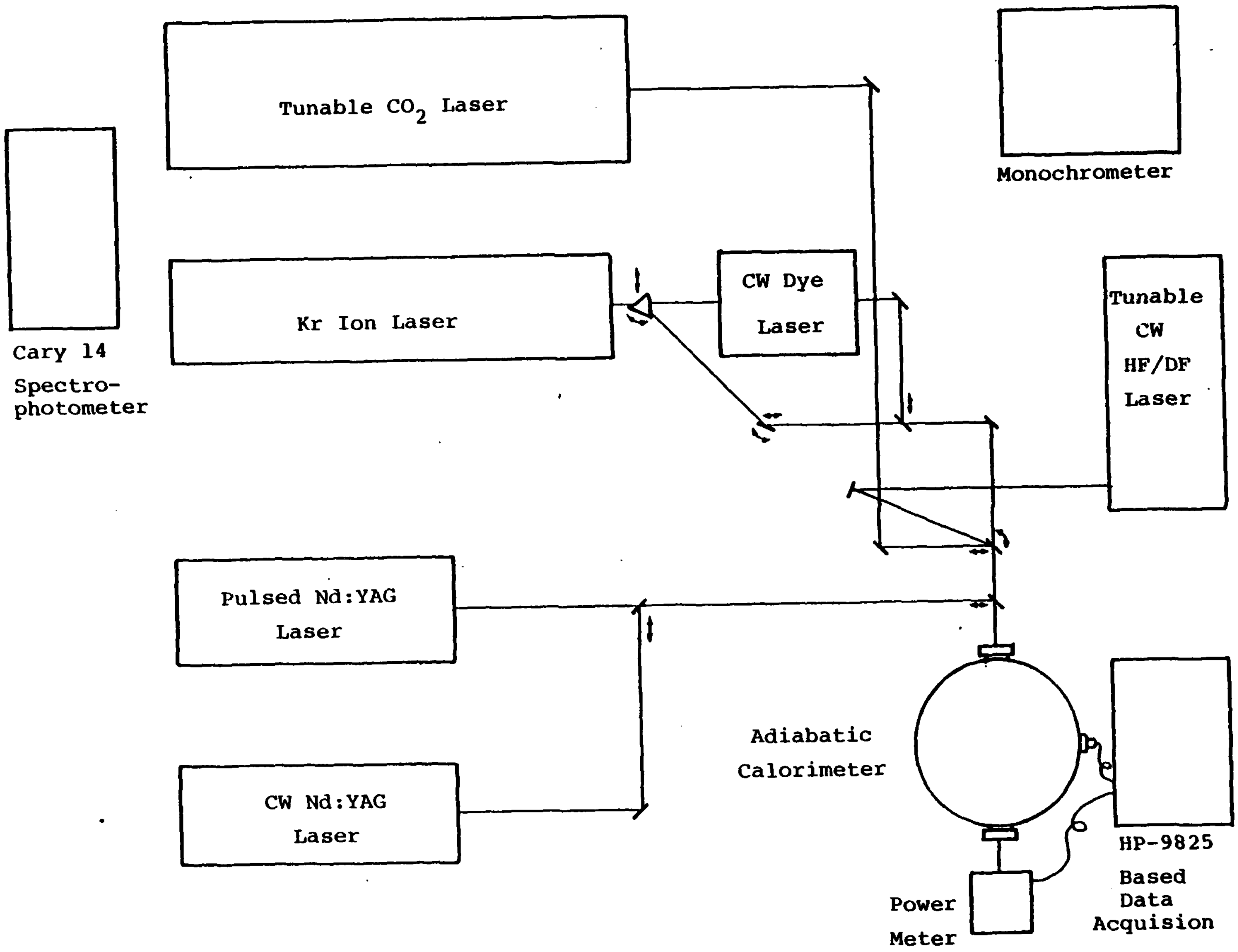

Figure 1. Laser Absorption Studies Laboratory: Optical Configuration

2.3 Materials (Susan Allen)

The materials obtained for optical and mechanical studies are listed in Table 1.

Composition	Vendor	Comments
CaF_2 + 1.0% Gd	Raytheon	Fusion cast, coarse-grains
CaF_2 + 0.1% Gd^{3+}	Optovac	Crystal
CaF_2 + 1.0% Gd^{3+}	" "	" "
CaF_2 + 1.0% Ce^{3+}	" "	" "
SrF_2 + 1.0% Gd^{3+}	" "	" "
BaF_2 + 1.0% Gd^{3+}	" "	" "
CaF_2 + Th^{3+}	Harshaw	Crystal window (< 1% Th^{3+})
CaF_2 + Dy^{3+}	" "	" " (< 1% Dy^{3+})
KCl + Eu^{2+}	" "	" "
KCl + Sr^{2+}	Raytheon	Crystal 73-82 (5000 PPM Sr^{2+})
KCl + Sr^{2+}	" "	" " 73-63
CaF_2	" "	Cast windows
NaF	" "	

Table 1: Alkali halides and alkaline earth halides for optical and mechanical studies

2.4 Absorption Results by Laser Calorimetry (M. Bass and S. Allen)

After the nearly one and one third years required to establish the optical absorption facility, experiments were initiated to measure the 10.6 and 1.06 μm absorption of samples of doped and undoped alkali halides, alkaline earth fluorides. The results of these measurements are listed in Table 2.

In addition the 2.7 μm absorption of CaF_2 (Sample # 1 in Table 2) was measured and found to be 4×10^{-4} cm^{-1}.

Table 2 : Absorption of Alkali Halides and Alkaline Earth Halides

Samples	CO_2 10.6 μ	YAG 1.06 μ
1) CaF_2 Raytheon	3.5	6.5×10^{-5} cm^{-1}
2) NaF	1.22	8.5×10^{-5} cm^{-1}
3) 1 % Gd/CaF_2	High*	6.8×10^{-3} cm^{-1}
4) 5000 PPM Sr^{++}/KCl Raytheon 73-82	4.0×10^{-3} cm^{-1}	3.6×10^{-4} cm^{-1}
5) Eu^{++}/KCl Harshaw	1.13×10^{-3} cm^{-1}	5.48×10^{-4} cm^{-1}
6) Th^{++}/CaF_2 Harshaw	High*	6.9×10^{-4} cm^{-1}
7) Dy^{+++}/CaF_2 Harshaw	High*	.45 cm^{-1}
8) Sr^{++}/KCl Raytheon 73-63		
2.45 cm long	5.2×10^{-3} cm^{-1}	3.3×10^{-4} cm^{-1}
1.65 cm long	3.3×10^{-3} cm^{-1}	1.5×10^{-4} cm^{-1}
.96 cm long	2.5×10^{-3} cm^{-1}	$.9 \times 10^{-4}$ cm^{-1}

---

*Too large to be measured

2.5 Vacancy Tracking by Color Centers Generated by Two Photon Absorption (H. Park and W. H. Steier)

The goal of this work was to study and understand the interaction of the optical and mechanical properties of pure and doped alkali halide crystals. These properties are correlated with point defects and vacancies of these materials. As a way, two photon excitation of electron-hole pairs was proposed as a mean of elucidating the point defect structure of these materials. If electrons or electron-hole pairs (i.e. excitons) are excited somehow (e.g. X-ray, electron-beam, or UV), electrons will be trapped at the negative ion vacancy site (holes at positive ion vacancy site) and produce color centers (F or U centers) in the crystal. The density and distribution of these color centers should be related to the density and distribution of the vacancies.

During this period we only dealt with F centers because they are relatively easy to generate and measure. The negative ion vacancy density should be proportional to the F-center concentration in the crystal as a first approximation and the F-Center concentration can be measured from the transmittivity of crystal at the absorption band (F-band)(1) In these experiments, a XeCl laser has been used to generate electron-hole pairs in alkali halide crystals by two photon absorption. Two photon energy of the laser (3080Å) is 8.06 eV. which is well within the absorption edge of some of alkali halide materials. The first absorption peak of NaCl, KCl and KBr are 7.96 ev, 7.76 and 6.77 eV respectively(2). These are exciton bands. The band-to-band transitions occur approximately 1 eV beyond the first absorption peak for most ionic crystals(3). For all three above crystals, color centers can be easily obtained with XeCl laser pulse energy less than 10mJ focused on 2 x 0.5mm (pulse width ~ 20 nsec).

For these measurements KBr single crystals from Harshaw Chemical Company were used. In KBr, bluish F centers were observed even with a 5mJ pulse, but on the other hand these crystals are so fragile that 3 or 4 shots of 30mJ pulses could easily damage the crystal. The absorption band of the F center in KBr was measured with a spectrophotometer and shown to be centered around 6300Å.(4) This wavelength conveniently allowed the use of the He-Ne laser to moniter F-center concentration in KBr. F-center concentration was measured as a function of input energy. Figure 2 shows the experimental set up. The XeCl laser beam is focused on a polished KBr window (5mm thick) through a quartz lens. The He-Ne laser beam is also focused and made to overlap with XeCl laser beam in the crystal. With each UV laser shot, F centers are created and the intensity of transmitted He-Ne laser is reduced. As time progresses after each shot, the trapped electrons at the F centers will escape by absorbing He-Ne laser photons or by thermal energy, the color centers diminish, and the crystal goes back to original state. Figure 3 shows the transmittivity change as a function of time. One can calculate the F center concentration in the crystal by using equation(5)

$$\alpha = 7.75 \times \frac{1}{H} \cdot \frac{(2 + n^2)^2}{n} \times 10^{-18} \cdot f \cdot N_0$$

where α : absorption coefficient

H : F center absorption bandwidth (0.34 ev for KBr)

n : refractive index (1.559 for KBr)

f : oscillator strength (0.85 for KBr)

N_0 : F center concentration

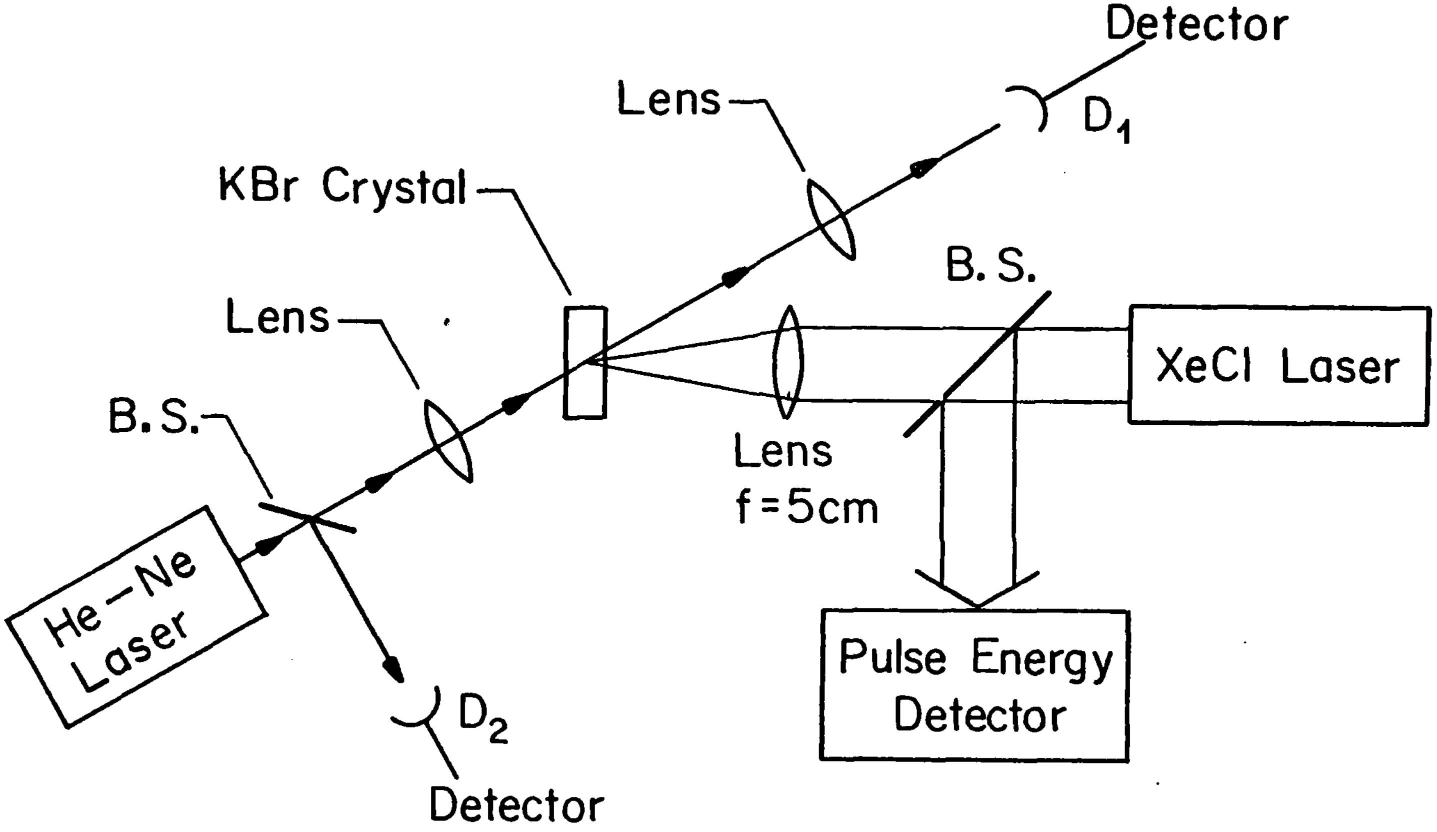

Figure 2 Transmittivity Measurement. Detector D_1 measures transmitted power and D_2 measures power fluctuation of He-Ne laser.

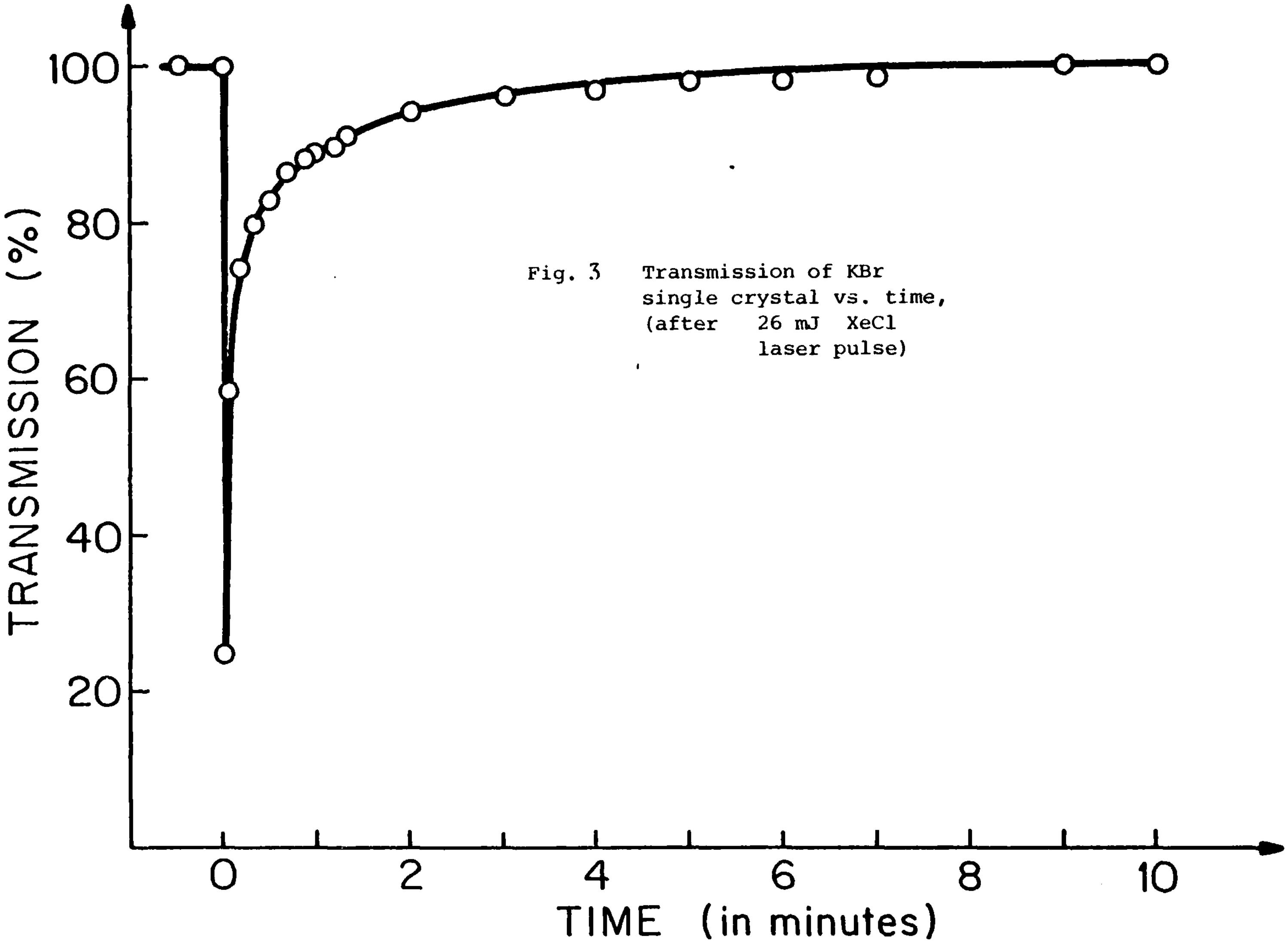

Fig. 3 Transmission of KBr single crystal vs. time, (after 26 mJ XeCl laser pulse)

At $t = 0^+$ after UV laser pulse, α is 13.68 cm^{-1} from the data which gives an F center concentration of 5.6×10^{16} cm^{-3} The decay time of color center is ~10 sec from this experiment.

In the next experiment, we attempted to determine if the F-center concentration can be related to the number of vacancy sites in the crystal.

In these preliminary experiments we attempted to vary the vacancy concentration by heating and quenching the samples. It is known that one can generate additional vacancy sites in a crystal by heating it close to the melting point, and that these vacancies can be frozen in by rapidly quenching the crystal. In this way one can increase the vacancy concentration in a crystal(6), however the excessive vacancies will, with time, diffuse to the surface of the crystal(7). In this experiment we measure the transmittivity of the crystal before and after quenching at $t = 0^+$ after exposure to the same UV energy (~9mJ)

The KBr crystal was held at 650°C for 20 minutes in a oven and then quenched to room temperature in oil. The transmission was measured at $t = 0^+$ as a function of time after the quench. The results are shown in Figure 4. Each circle is the average value of 5 measurement at different spots of the crystal.

From the data we can conclude that up to 1/2 hour after quenching the transmittivity (or F center concentration) is different from that before the heating and quenching but after one hour the transmittivity has returned to its original value. The transmittivity change is ~3% which is marginally greater than our experimental error. In another experiment with another KBr crystal, the transmittivity decreased by ~5% up to 1-1/2 hours after the quench.

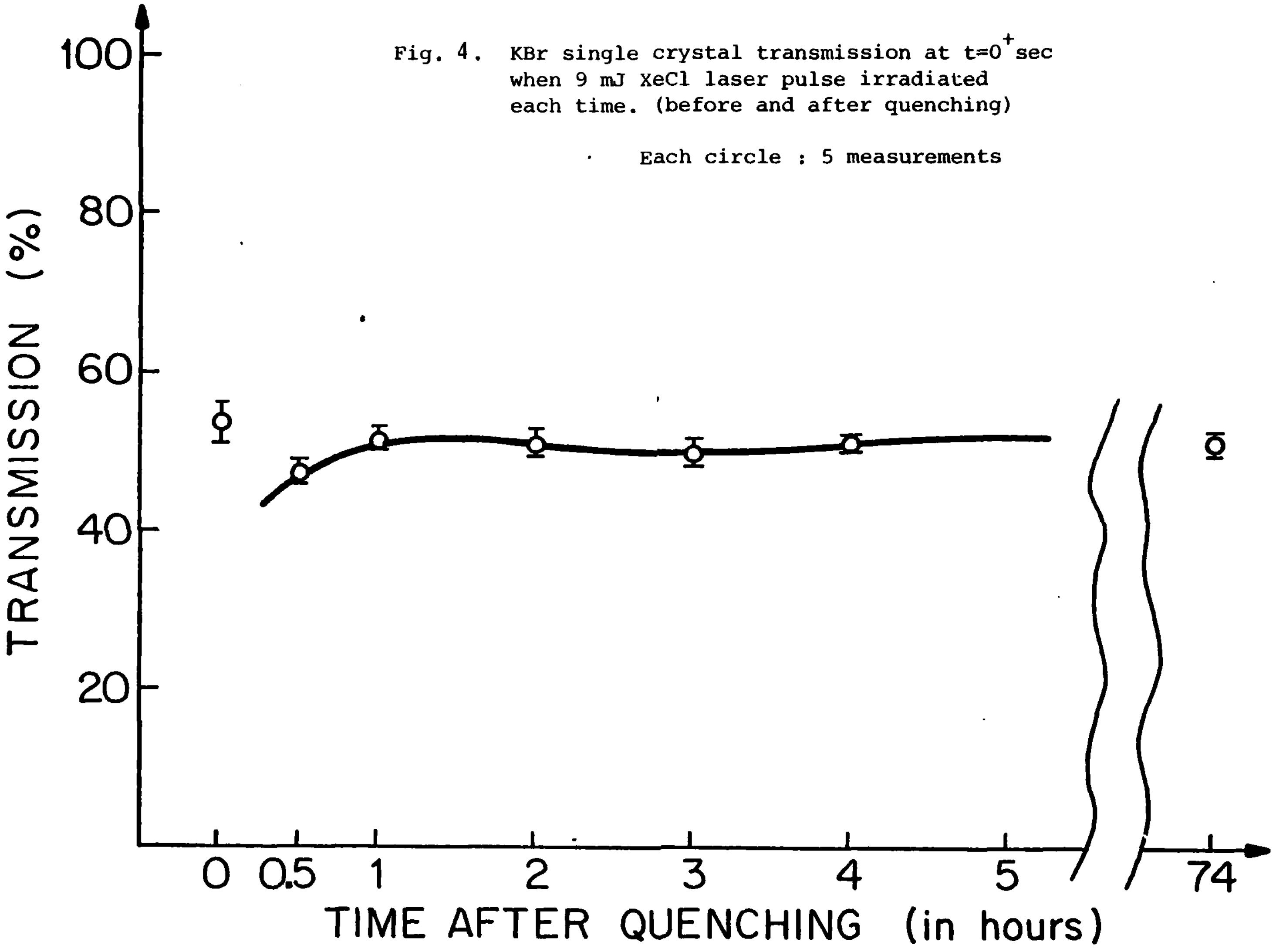

Fig. 4. KBr single crystal transmission at $t=0^+$ sec when 9 mJ XeCl laser pulse irradiated each time. (before and after quenching)

Each circle : 5 measurements

We can tentatively interpret our results to confirm the relationship between vacancy density and color center density, however other factors must also be considered. For example, it is known that in crucible grown KI the color center density is a function of previous irradiation and plastic deformation, however, other work has shown this not to be important in KBr.(8)

These preliminary experiments appear to be successful but considerable more work remains to show that the color center density is a valid measure of vacancy density.

References

1. L.F. Mollenauer, G.C. Bjorklund and W.J. Tomlison, Phys. Rev. Lett. 35, 1662 (1975).
2. M. Geller, D.E. Altman, and T.A. DeTemple, Appl. Phys. Lett. 11, 221. (1967).
3. A.J. Dekker, Solid State Physics, Prentice Hall, 1957, p 373.
4. F. Seitz, Rev. Mod. Phys. 18, 384 (1946).
5. J.J. Markham, F-centers in Alkali halides, Academic Press N.Y. 1966, p 31.
6. R.O. Simmons and R.W. Balluffi, Phys. Rev. 117, 52 (1960).
7. C. Kittel, Introduction to Solid State Physics 2nd ed. John Wiley & Sons, N.Y. 1956, p 487.
8. J.H. Parker, Jr., Phys Rev. 124, 703, (1961).

2.6 Optical and Mechanical Properties of Alkali Halides and Alkaline Earth Fluorides (S. M. Copley and J. Savage)

Because so little research had been done on the effect of doping on the mechanical properties of the alkaline earth fluorides, it was decided to initiate work on this type of material. Alkali halide specimens were also obtained, see Table 1, however, only optical measurements had been carried out on these specimens at the time this program terminated.

The goal of this research was to determine by hardness and absorption measurements (both I.R. and U.V.) whether thermal treatment could be used to harden alkaline earth fluorides through the formation of point defect complexes without producing an increase in I.R. absorption. The U.V. absorption measurements were to be carried out as a means of detecting defect complex formation.

Experiments were initiated on CaF_2 + 1.0%Gd^{3+} deformed bend specimens provided by Raytheon. The specimens had been originally been cut from fusion cast ingots and were very coarse-grain polycrystals.

An initial experiment was carried out on an as-received specimen to determine the amount of scatter that could be expected in a series of hardness measurements. A traverse was made along one face of a specimen. Indentations were made with the long dimension either parallel to or perpendicular to the long dimension of the specimen. The measurements were made over a period of 40 days to detect any change with time. The best estimate of the population mean and standard deviation was 214.4 and σ = 5.6, respectively, for the transverse measurements and μ = 201.6 and σ = 1.4 respectively for the longitudinal measurements. It was concluded from these measurements that the scatter was small enough so that hardness could be used to measure any significant change in yield stress and that neither location along the specimen nor time produced any systematic variation in hardness.

To investigate the effect of thermal treatment, specimens were annealed at 625°C to dissociate all point defect complexes, quenched and then aged. It was hoped that the quench would be rapid enough to preserve the point defects in a dissociated state but that the defects would form complexes upon aging resulting in an increase in hardness. It was found, however, that direct quenching into oil was not possible because of extensive cracking due to thermal stresses. Consequently, experiments were carried out in which the specimen was sealed in a fused quartz capsule during oil quenching.

Table 3 shows the results of several quenching experiments. Each hardness value is the average of five independent determinations. Although the results are not entirely consistent, it appears that annealing and quenching increases hardness. This suggests that the quench was not sufficiently rapid to suppress the formation of hardening point defect complexes.

Although it was originally intended to age the quenched specimens at a temperature greater than room temperature, it was discovered that changes in hardness occurred during room temperature aging. Typically, the hardness decreased initially

Sample	As-Received (KHN)		Quenched (KHN)	
	L	T	L	T
9 a	242	215	262 (+20)	265 (+50)
13 a	226	242	222 (-4)	195 (-47)
14 a	227	232	216 (-11)	240 (+8)
15 a	204	204	229 (+25)	238 (+34)
16 a	216	214	223 (+7)	218 (+4)
17 a	208	227	225 (+17)	226 (-1)

Table 3: Knoop hardness of various specimens in as-received and quenched conditions. The letter L indicates that long axis of indent was parallel to the long axis of the specimen; T indicates that the long axis of the indent was perpendicular to the long axis of the specimen.

and then increased passing through a maximum at about 50 hours.

The scatter in results of the quenching experiments as well as the occurrence of "hardness reversals" in the aging curves suggests that the Raytheon samples may include several grains. In this case, deviations from normal behavior could be attributed to an orientation effect or to the nearness of the indentation to a grain boundary.

Preliminary examination of the UV spectra of the Raytheon specimens after quenching and agin produced no evidence for defect complex formation. Thus while we have shown that thermal treatment may increase the hardness of Gd^{3+} doped CaF_2 at room temperature, at least temporarily, we have not been able to link the hardness increase with the formation of any specific defect.

2.7 Optical and Mechanical Properties of ZnSe (W. G. Spitzer and J. S. Ko)

A manuscript describing the results of this work has been prepared for submission to the Journal of Applied Physics . A copy of this manuscript is attached to this report in Appendix B.

2.8 Evaporation Driven Liquid Sintering

In this project, the feasibility of applying a new process, evaporation driven liquid sintering (EDLS) to the sintering of MgF_2 was investigated. Sodium chloride was selected as the volatile liquid sintering aid. Magnesium fluoride powder compacts containing NaCl were heated in a controlled atmosphere to suppress evaporation of NaCl. After sintering has occurred, the NaCl must be evaporated from the compact.

It has been shown that for the evaporation driven liquid sintering process to be successfully applied, the volatile liquid must completely wet the the powder being sintered and the powder being sintered must have limited solubility in the volatile liquid. Neither of these conditions were satisfied by the NaCl. Before another sintering aid could be found, the student working on this project left the University.

Reference

V. V. S. Rana, S. M. Copley, and J. M. Whelan, "Sintering of Powder Compacts with a Volatile Liquid Phase (MgO-LiF)", Chapter in Ceramic Microstructures '76, R. M. Fulrath and J. A. Pask, eds. Westview Press, Boulder CO. (1977).

2.9 Measurements of Electrical Conductivity at High Temperatures of MgO Single Crystals Doped with Transition Metals and/or Lithium (F. A. Kröger and Bu-Chin Chung)

MgO is a mixed conductor the properties of which are strongly affected by aliovalent dopants such as Fe, Mn and Li. The contributions by ionic and electronic components to the current can be determined by combining measurements of total conductivity with transference numbers t_i and $t_{el} = 1 - t_1$ determined from emf measurements on cells of the type:

$$\mathrm{Pt},O_2\ (P_{O_{2,I}})/\mathrm{MgO}/\mathrm{Pt},O_2(P_{O_2})_{II}$$

the emf of which is given by:

$$E = \frac{RT}{4F} \int_{I}^{II} -t_i\ d\ \ln P_{O_2}$$

Transference numbers at $(P_{O_2})_{II}$ are therefore found from the slope of a curve $\frac{4FE}{RT}$ versus $(P_{O_2})_{II}$ with $(P_{O_2})_I$ constant:

$$(t_i)_{II} = \frac{4F}{RT} \quad (\partial E/\partial \ln(P_{O_2})_{II})_{(P_{O_2})_I}$$

and $$\sigma_i = \sigma_{t_i}, \quad \sigma_{el} = \sigma\ (1-t_i)$$

A high temperature furnace with super Kanthal heating elements and Zircon insulation was built, a gas train for mixing gases required for establishing oxygen pressures between 10^{-10} and 1 atm was constructed, and measuring equipment was assembled. Owing to personnel problems, no measurements were done before the contract expired.

3. PUBLICATIONS

Michael Bass, Eric W. Van Stryland and A. F. Stewart, "Laser Calorimetric Measurement of Two-Photon Absorption", Appl. Phys. Lett. 34, 142-4 (1979).

W. G. Spitzer and J. S. Ko, "Localized Vibration Modes of Li and Al in ZnSe", (in preparation).

S. M. Copley and S. Allen, "Optical and Mechanical Properties of Gd-doped CaF_2", (in preparation).

H. Park and W. H. Steier, "Vacancy Tracking by Color Centers Generated by Two Photon Absorption", (in preparation).

4. PERSONNEL

Principal Investigator:	S. M. Copley
Senior Investigators:	M. Bass
	F. A. Kröger
	G. H. Narayanan
	W. G. Spitzer
	W. H. Steier
Research Scientists:	S. D. Allen
	R. Sheftall
	V. V. S. Rana
	H. Sankur
	H. Park
	R. T. Swimm
	R. Quimby
	N. Koumvakalis

Research Assistants:

- A. Stewart
- J. S. Ko
- A. Halliyal
- T. R. Gururaja
- B. C. Chung
- S. T. Wu

APPENDIX "A"

Laser calorimetric measurement of two-photon absorption

Michael Bass, Eric W. Van Stryland, and A. F. Stewart

Center for Laser Studies, University of Southern California, Los Angeles, California 90007

(Received 21 August 1978; accepted for publication 24 October 1978)

A laser calorimeter has been used to measure two-photon absorption in solids. This new technique provides greater sensitivity than is possible in nonlinear transmission measurements. The two-photon absorption coefficients of CdTe and CdSe at 1.06 μm using ~16-nsec (FWHM) pulses are 0.13 ± 0.04 and 0.050 ± 0.014 cm/MW, respectively.

PACS numbers: 42.10.Ke, 78.20.Dj, 42.60.–v

The laser calorimeter is a device that is widely used to measure small linear absorptions at wavelengths where laser sources are available. Such an instrument can measure absorptions which are less than one part in 10^5 using a 1-W laser.[1] The calorimeter measures the total absorption due to all processes including the intensity-dependent phenomenon of two-photon absorption (TPA). Thus, the experimental technique described in this paper is based on a measurement of the total absorption as a function of the laser intensity. Calorimetric measurements of the total absorption in CdTe and CdSe as functions of 1.06-μm laser intensity were used to obtain both linear and TPA coefficients of these materials. The results can be understood by using a simple model for the attenuation with distance in the presence of TPA and by properly accounting for multiple reflections in the sample.

In 1931, M. Göppert-Mayer presented a theoretical description of TPA in which the transition probability was shown to be proportional to the square of the light intensity.[2] Thus, a material having both linear and two-photon absorption will transmit light according to the expression

$$\frac{dI}{dZ}(x,y,z,t) = -[\alpha + \beta I(x,y,z,t)]I(x,y,z,t). \qquad (1)$$

Here, $I(x,y,z,t)$ is the light intensity in MW/cm^2 and is a function of the space coordinates and time, z is the direction of propagation, α is the linear absorption coefficient in cm^{-1}, and β is the two-photon absorption coefficient in cm/MW. In many materials of interest α will be small, $\alpha \simeq 10^{-2}$ cm^{-1}, and $\beta \simeq 10^{-2}$ cm/MW according to the transmission measurements at high intensities.[3] Thus, a modest intensity of 1 MW/cm^2 will result in a two-photon contribution to the total absorption which is equal to the linear term [see Eq. (1)]. On the other hand, this intensity will result in a change in transmission for samples shorter than 1 cm of less than 1%, which is too small to be measured accurately. A comparison of the two techniques can be made by noting that in a transmission experiment one measures a small change (the reduction of transmission due to TPA) in a large quantity (transmitted intensities), whereas using calorimetry one measures a large change (the added absorption due to TPA) in a small quantity (total absorption).

The experimental procedure is to measure the total absorption as a function of intensity and evaluate the data according to Eq. (1), taking into account reflections at the rear surface. A flashlamp-pumped *Q*-switched, TEM$_{00}$ mode Nd : YAG laser was the source for the experiments, as shown in Fig. 1. The laser was operated at ~5 Hz with an output of ~1 mJ/pulse.[4] The pulse temporal waveform was a Gaussian function with full width at $1/e$ points in intensity of 19 nsec. A beam scan was used to determine the spatial profile which was Gaussian, having a $1/e$ full width in intensity of 1.2 mm at the focusing lens. An 8-cm focal length lens was used to increase the intensity at the samples, which were placed 4 cm behind the focus. The attenuators and optics in front of the sample limited the maximum peak-on-axis intensity at the sample to ~30 MW/cm^2, with an average power of approximately 5 mW. The energy per pulse was measured by averaging the output of over 100 pulses with a pyroelectric joulemeter. The accuracy of the TPA measurements is sensitive to pulse-to-pulse energy variations, which

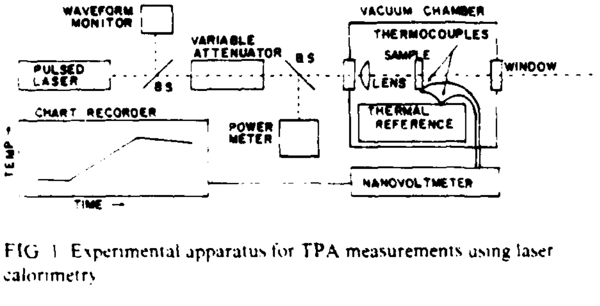

FIG. 1. Experimental apparatus for TPA measurements using laser calorimetry.

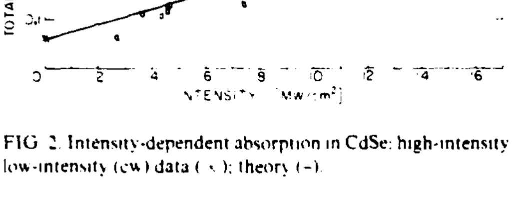

FIG. 2. Intensity-dependent absorption in CdSe: high-intensity data (□'s); low-intensity (cw) data (○); theory (–).

0003-6951/79/020142-03$00.50

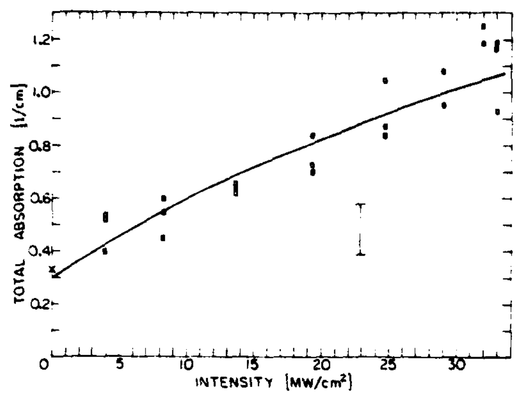

FIG. 3. Intensity-dependent absorption in CdTe: high-intensity data (I's); low-intensity (cw) data (×); theory (–).

must therefore be kept as low as possible (~5%). The beam intensity at the sample was adjusted using a two-polarizer attenuator described in Refs. 5 and 6.

A thermocouple attached to the otherwise thermally isolated sample recorded the sample's temperature change due to the absorption of the laser light. When amplified and recorded, the thermocouple voltage appeared as shown on the chart recorder in Fig. 1. While the laser is on the temperature rises. The gentle slopes while the laser is off are due to small thermal losses that are seen with thin samples. The time constant of the calorimeter was long enough so that a 5-Hz laser beam caused no uneveness in the recorded temperature change. Thus, the calorimeter responded to the total average power absorbed. The calorimeter was of conventional design and, when evacuated, had a measured sensitivity to absorption of one part in 10^5 with a 1-W source.

Data such as in Fig. 1 was obtained at several laser intensities for room-temperature samples of CdTe and CdSe. The samples were single crystals, and the CdSe was oriented with its optic axis normal to the entrance (exit) surface. This orientation eliminated the possibility of second-harmonic generation at 0.53 μm which could be directly absorbed. The CdTe sample had its optic axis approximately 22° away from the normal to the entrance surface. Figures 2 and 3 show the intensity dependence of the total absorption of these two materials measured calorimetrically. For a small total absorption [i.e., $(\alpha + \beta I)z \ll 1$], Eq. (1) predicts a straight line for absorption versus intensity. The vertical intercept of this line gives α and its slope determines β. In these experiments which employ a Gaussian beam profile and a Gaussian temporal shape, the TPA coefficient would be $2\sqrt{2}$ times the slope in such a plot. The data fits a straight line quite well, but the total absorption at the highest intensities used for CdTe was over 20%. Thus, Eq. (1) must be solved exactly. This was done previously, including the effects of Gaussian spatial and temporal profiles, but the effects of multiple reflections were neglected.[3] For high-index materials, the intensity of the reflected beam from the rear surface can significantly affect the computed absorption coefficients. Since TPA results from the imaginary part of the third-order optical nonlinear susceptibility $\chi^{(3)}$, the field equations for both the incident and reflected beams were used to obtain the following coupled differential equations for the intensities:

$$\frac{dI}{dz} = -[\alpha + \beta(I + I_R)]I,$$

$$\frac{dI_R}{dz} = +[\alpha + \beta(I + I_R)]I_R,$$

where I is the intensity of the incoming beam and I_R is the intensity of the reflected beam. Subsequent reflections have been neglected because they contribute still less to the total absorption. Noting that the product $I(z)I_R(z)$ is a constant everywhere in the sample, these equations can be solved in closed form with the constant as a parameter. A rapidly converging numerical iterative procedure for determining the constant from the boundary conditions was used to determine the total absorption integrated over the spatial and temporal beam profiles.

The theoretical fits along with the data are shown in Figs. 2 and 3. These fits were used to obtain the values for β listed in Table I. The values given for α were obtained using a cw Nd : YAG laser and the usual calorimetric technique. These measured values of α are quite accurate and as such were used in the calculations of β. This means that the values of β given in Table I are the result of a one-parameter fit. The deviation of the fit from the data at high intensities, particularly for CdSe, may be due to a contribution from direct absorption by two-photon-created free carriers, as discussed in Refs. 3 and 7. However, at this time the data is insufficient and the error bars too large to make any conclusions concerning the possible role of free carriers. Work is continuing in this area seeking a predicted pulse width dependence to TPA if free-carrier absorption is significant.

The experimental error bars shown in Figs. 2 and 3 were determined from scatter in the data and uncertainties in determining the heating rate from curves such as sketched on the chart recorder in Fig. 1. The laser-intensity fluctuations, the accuracy of the laser-spot-size measurement, and temporal profile measurement along with the uncertainties mentioned above combine to give the quoted accuracies in Table I. The accuracy of TPA measurements using laser calorimetry has the potential for considerable improvement. The initial work presented here has, however, demonstrated the feasibility of the technique.

The inclusion of the reflected beam in the analysis of TPA measurements is essential in high-index materials, where it has been ignored previously,[3] but may be eliminated in future experiments (thus greatly simplifying the calculations) by using AR-coated samples. It should be pointed out

TABLE I. Linear absorption coefficient α and two-photon absorption coefficient β at 1.06 μm.

Material	α (cm)	β (cm/MW)
CdSe	0.062 ± 0.06	0.050 ± 0.014
CdTe	0.335 ± 0.03	0.130 ± 0.036

that in certain materials the two-photon excited level can decay through a combination of radiative and nonradiative processes. Then, part of the total TPA may not register as heat generated in the sample. This means that a simultaneous transmission measurement may make it possible to determine the quantum efficiency of such radiative transitions. This type of quantum efficiency study and measurements of TPA using two different lasers are in progress.

The partial support of the Air Force Office of Scientific Research under Contract No. F49620-78-C-0065 is gratefully acknowledged. Valuable help in calorimetric measurement techniques was provided by Dr. S.D. Allen and Dr. J.-C. Diels provided a turbine-driven Q-switch for the Nd : YAG laser as well as valuable theoretical help.

[1] A. Hordvik, Appl. Opt. **16**, 2827 (1977).

[2] M. Goppert-Mayer, Ann. Phys. (Leipzig) 9, 273 (1931).

[3] J.H. Bechtel and W.L. Smith, Phy. Rev. B **13**, 3515 (1976).

[4] For CdTe the pulsed repetition frequency was 6.7 Hz and for CdSe the pulsed repetition frequency was 7 Hz. The CdTe sample was 2.03 mm thick and the CdSe sample was 0.89 mm thick.

[5] M. Bass, *Laser-Induced Damage to Nonlinear Crystalline Materials*, NBS Special Publication 341 (U.S. GPO, Washington, D.C., 1970).

[6] K.M. Leung, M. Bass, and A.G.J. Balbin-Villaverde, *Damage to* 10.6*μm Window Materials Due to* CO_2 *TEA Laser Pulses*, NBS Special Publication 435 (U.S. GPO, Washington, D.C., 1975).

[7] F. Brynkner, V.S. Dneprovskii, and V.U. Khattatov, Sov. J. Quantum Electron. **4**, 12 (1974).

APPENDIX "B"

I Introduction

There has been a long-standing interest in the optical properties of ZnSe, particularly the luminescent characteristics and their relationships to impurities and native defects. Some defect models have been suggested, but the microscopic structure is not yet completely clear. Recently the importance of ZnSe as an infrared window material for high power laser applications demonstrated the need more detailed studies of the microstructural features of the defects and their relationships to the infrared absorption.

It is now well[1] established that if the mass of a substitutional dopant is sufficiently small compared to those of the host atoms, such as Al or Li in ZnSe, then infrared absorption measurements of the localized vibrational modes (LVM) are a very useful diagnostic tool in helping to understand the nature of the defect. An analysis of the infrared spectra can give important information about the microstructure and symmetry properties of the defects and impurity atom positions in the crystal lattice. Lithium, with its light mass and fast diffusion rate has played a particularly important role in LVM studies of several defects. Li diffused into GaAs[2] can be a n-type or a p-type impurity, and can sit at an interstitial site, at a substitutional site, or in the form of complexes. Another physical property which is impurity dependent is the hardness of materials. It is known[3] that hardening of Si-doped GaAs is produced by the interaction of the solute-vacancy pairs with the moving dislocations. Because of the IR window application, there is considerable interest in hardening mechanisms in ZnSe. If one labels the defects by their LVM, then one can determine whether the hardness of ZnSe is a function of impurity concentration and if so, how the hardness depends upon the concentration of specific impurity-related defects.

This is a report of the progress in a study of the optical and mechanical properties of ZnSe, and it includes:

1) Localized vibrational mode absorption and hardness studies of Al-doped ZnSe. Both properties are measured as functions of impurity concentration and annealing conditions.
2) A LVM study of lithium diffused ZnSe which is initially undoped or doped with n-type impurities (Al, Ga).

II Experimental Method

The ZnSe ingots used in this study were purchased from Eagle-Picher Co. The crystals were grown under an inert gas pressure by using a modified Bridgeman technique. The ingots are polycrystalline with large grain size with the size depending somewhat upon the dopant and its concentration. The dopants and their concentrations in the material we have used are as follows (values given by the supplier[4]):

(1) undoped ZnSe

(2) Al doped ZnSe: 100 ppm and 300 ppm

(3) Li doped ZnSe: 100 ppm

(4) Ga doped ZnSe: 100 ppm and 3000 ppm

(5) In doped ZnSe: 40 ppm and 400 ppm.

The group III elements Al, Ga and In are expected to be n-type dopants in ZnSe. The impurities are known to be substitutional on the Zn sublattice and form shallow-state, effective mass-type donors. Very little is known about the nature of Li as an impurity in ZnSe. An acceptor state associated with Li_{Zn} has been identified[5], however the behavior of Li in ZnSe is likely to be complicated and involve more than one type of defect species. The as-grown crystals are highly self-compensated and have no detectable free carrier absorption.

We used the most heavily Al-doped ZnSe (300 ppm) in a number of annealing experiments in which the Se pressure is controlled. The samples were cut to a size of about 12 x 5 x 0.3 mm^3, lapped, and then mechanically polished. After subsequent cleaning, the samples were sealed in evacuated quartz ampoules containing Se shot. The ampoule was placed in a two zone furnace with the crystal at one end of the ampoule which was in the center of the main furnace. The Se pool was at the other the of the ampoule which was placed in the center of the 2nd furnace. The temperature of the main furnace was set at 900 K. The Se partial pressure was controlled by adjusting the temperature of the secondary furnace. After annealing, the sample was lapped again on both sides, reduced to a suitable thickness, and chemically polished.

Infrared absorption measurements were made at liquid nitrogen temperature by using a Perkin-Elmer model 210 single-beam grating spectrometer. The frequency range was from $\nu \sim 500\ cm^{-1}$ to $\sim 300\ cm^{-1}$ and the typical thickness of the samples measured was 8 mils (0.2 mm). The absorption coefficient α was calculated from the transmission, T, and the reflectivity, R, by using the usual expression for a solid sample.

The lithium diffusion was carried out from an alloyed layer by the same technique as used previously for GaAs. In brief, thick samples were surface alloyed with a mineral-oil suspension of fine Li powder at 500°C in an argon atmosphere. A piece of undoped, highly polycrystalline ZnSe which was grown by Raytheon Corp. was used to provide the alloy pieces used in the diffusion process. The diffusion was carried out by sandwiching the samples between the alloyed pieces. The diffusion temperature was between 600°C and 800°C. For most samples, the time and temperature used for the diffusion is essentially the same, independent of dopant and concentration, about three to four hours at 700°C. As will be discussed there is evidence that one Li defect species does increase with longer diffusion times and therefore a Li saturation condition was not achieved. Samples diffused at 800°C for longer than two hours are heavily damaged. Often the central piece in the sandwich was fused to the alloy piece or the pieces became very brittle. After diffusion annealing, the samples were lapped and polished in the usual manner and the infrared transmission was measured.

Hardness measurements were carried out for some samples with a "Tukon Tester" by using a Knoop diamond indentor loaded with a 50 gm weight. Samples with chemically polished surfaces were used. Indentations were made on the central area of each grain to minimize the grain boundary effect. For samples which were annealed, the hardness was measured before and after repolishing the surface and no change was observed.

III. Results

A) Annealing of ZnSe:Al

The infrared absorption spectra of ZnSe:Al was first studied by Mitsuishi et al.[6] Six local modes were observed due to the presence of Al as shown in Fig. 1 for a sample having an Al concentration of ∿ 300ppm. The LVM studies by Mitsuishi et al. of absorption as a function of Al concentration and of ZnSe:Al annealing in a Se-rich atmosphere indicated a different behavior for the intensity of one of the bands which has its absorption peak at $\nu = 359\ \mathrm{cm}^{-1}$. This band was attributed to the $\mathrm{Al}_{\mathrm{Zn}}$ defect, where X_y means X occupying a y atom site. The source of the other five Al-related bands remains unresolved. Later experiments studying ZnSe:Al counterdoped with Cu, Ag, and Au also confirmed the different character of the $359\ \mathrm{cm}^{-1}$ band and supported the $\mathrm{Al}_{\mathrm{Zn}}$ idendification.

Mitsuishi et al. attempted to obtain more information about the Al-related bands by studying the annealing ZnSe:Al in a Se-rich atmosphere. Mitsuishi et al. annealed ZnSe:Al at 900°C for 120 hours with a Se pressure of 2 atms. All of the Al-related bands disappeared except the $359\ \mathrm{cm}^{-1}$ band. They attributed this result to the outdiffusion of the Al.

In the present study the annealing experiments were repeated under the same conditions except shorter annealing times were used. Figure 1 shows the absorption spectrum of ZnSe:Al (300ppm) before annealing, after aging for 40 hours and 80 hours at 900°C with a Se pressure of 2 atms. The $359\ \mathrm{cm}^{-1}$ band increases initially during the first 40 hours of annealing and then remains unchanged through the remaining heat treatment. The five unknown bands all decrease with annealing time. Additional annealing experiments under different annealing conditions show the same pattern with the amount of change depending on the temperature and Se pressure.

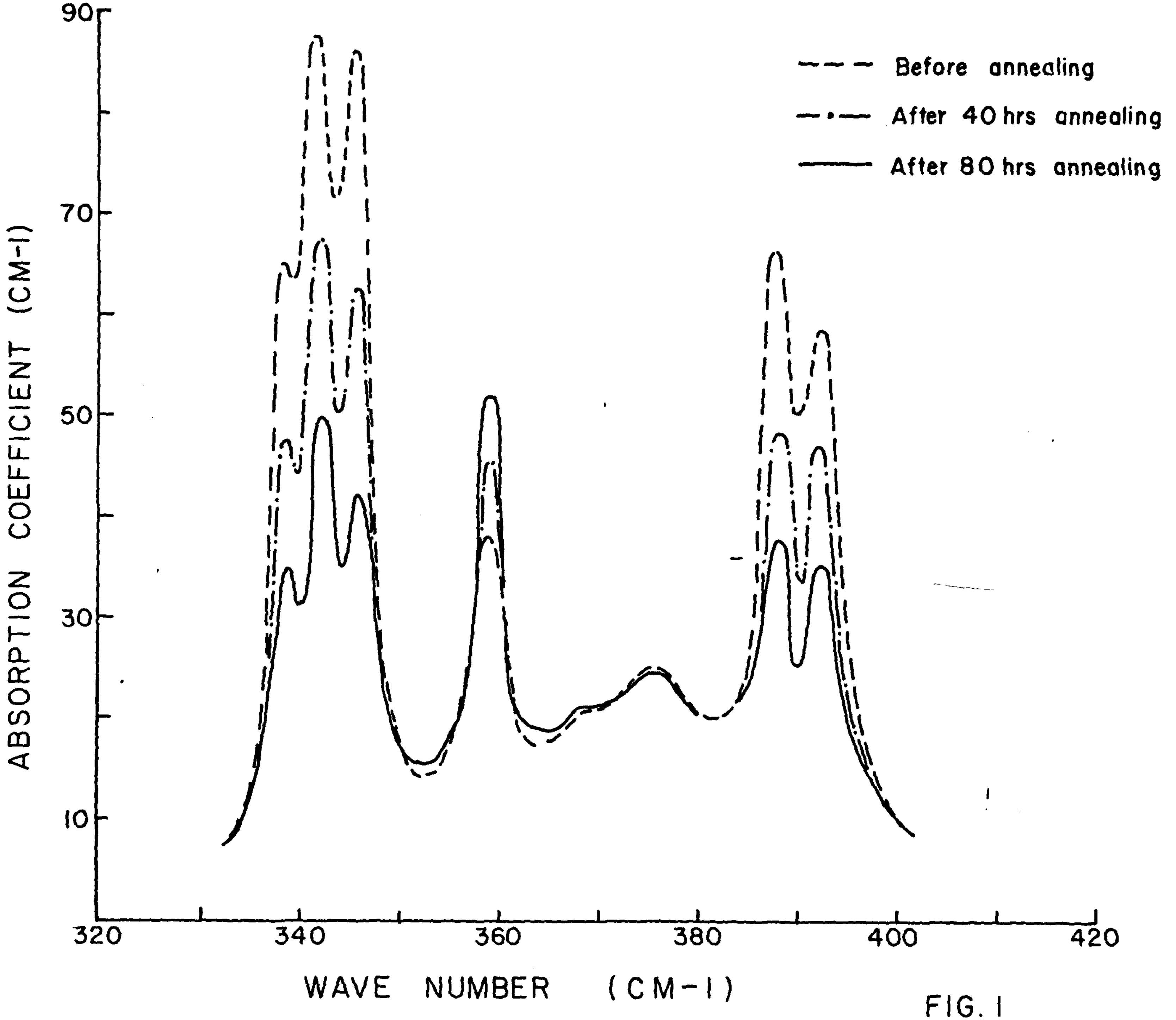
90
70
50
30
10
ABSORPTION COEFFICIENT (CM-I)
320
340
360
380
400
420
WAVE NUMBER (CM-I)
Before annealing
After 40 hrs annealing
After 80 hrs annealing

FIG. I

B) Undoped, Li diffused ZnSe

Infrared studies of ZnSe which were doped with Li during crystal growth have been reported by Mitsuishi et al.[8] Figure 2-(a) and 2-(b) are approximate line spectra indicating the frequencies and strengths of the absorption bands observed by them. They identified four ^{7}Li bands and two ^{6}Li bands as indicated by the arrows. They proposed that the other bands between $\nu = 450$ cm^{-1} and $\nu = 345$ cm^{-1} are the result of defect-induced enhancement of the usual two phonon lattice bands and therefore did not consider them further. They assigned the bands at $\nu = 336$ and 328 cm^{-1} to ^{7}Li defect modes and the corresponding bands at $\nu = 350$ and 341 cm^{-1} to ^{6}Li modes. The isotope frequency ratio is 1.04 which is small compared with 1.072 for Li in GaAs. This observation would indicate that the local modes of Li in ZnSe consist of vibrations of polyatomic complexes containing Li and a significant portion of the kinetic energy of each mode is not in Li motion. This result is unlike that for the modes in Li-diffused GaAs which consist primarily of Li vibrations.

We used the technique described in the experimental section to diffuse Li into ZnSe. In the Eagle-Dicher Co. material, which was diffused at 700°C for 4 hours, we observed six new ^{7}Li bands with peak absorption frequencies of ν = 420, 412, 389, 359, 350 and 343 cm^{-1} as well as their corresponding bands for ^{6}Li at ν = 451, 441, 419, 385, 375 and 367 cm^{-1} (see Figures 2 (c) and 2(d)). The isotope frequency ratio is 1.072 which is the same as that of Li-diffused GaAs and close to 1.080 for a purely Li harmonic oscillator. This shift indicates that the local modes which we have observed consist primarily of Li vibrations. The ^{7}Li band at $\nu = 420$ cm^{-1} as well as the ^{6}Li bands at $\nu = 441$ and 419 cm^{-1} fall on the strong two-phonon lattice absorption bands but the dramatic increase in the absorption co-

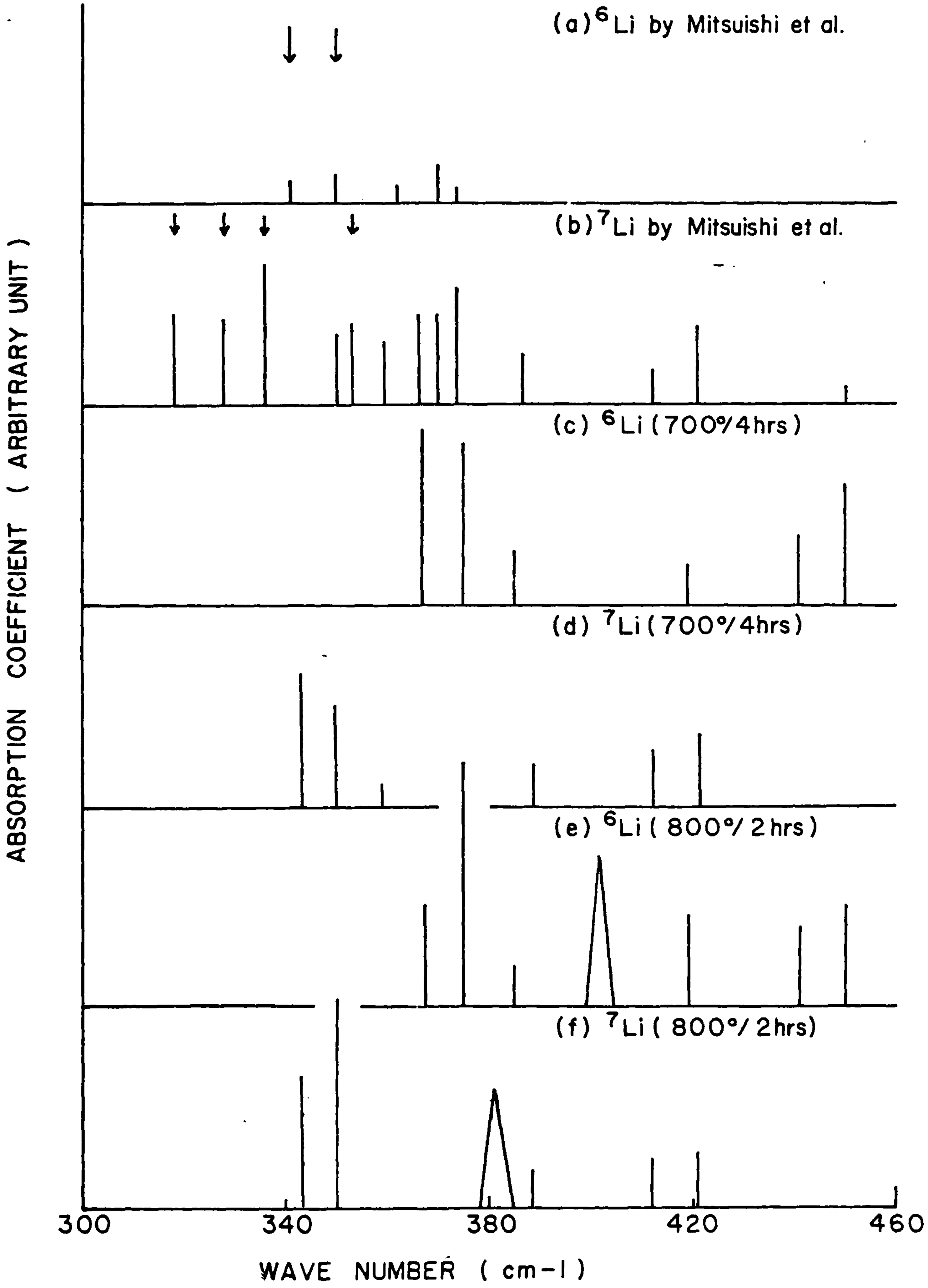
(a) ^{6}Li by Mitsuishi et al.
(b) ^{7}Li by Mitsuishi et al.
(c) ^{6}Li (700°/4hrs)
(d) ^{7}Li (700°/4hrs)
(e) ^{6}Li (800°/2hrs)
(f) ^{7}Li (800°/2hrs)
ABSORPTION COEFFICIENT (ARBITRARY UNIT)
300
340
380
420
460
WAVE NUMBER (cm-1)

FIG. 2

efficients and the presence of the isotopic counterparts make it clear that these are LVM bands and not an enhancement of the ZnSe two-phonon absorption process. We also observed two additional weak ^{6}Li bands at ν = 339 and 326 cm^{-1}. The corresponding ^{7}Li bands are not observed, probably because the frequencies are lower than 320 cm^{-1} where the lattice absorption increases rapidly with decreasing frequency making observation of LVM absorption bands very difficult.

In the samples diffused at 700°C for 16 hours rather than the 3 h used above, the result is the same except the ^{7}Li (^{6}Li) band at ν = 350(375) cm^{-1} has grown substantially with respect to the other LVM bands. The other bands retain their same relative strengths and show little, if any, change. In some cases the changes were difficult to measure accurately because relatively weak bands were close to strong ones or nearly coincided with strong two-phonon peaks.

When samples were diffused with ^{7}Li at 800°C for one or two hours the 350 cm^{-1} band increased dramatically. A very strong and broad band at ν between 380 and 390 cm^{-1} also appears (see figures 2 (e) and 2 (f)). The rest of the bands at ν = 420, 412 and 343 cm^{-1} show either some small growth or no change. The ^{6}Li diffused samples also show a large increase of the corresponding band at ν = 375 cm^{-1} and the presence of the broad band at ν between 400 and 410 cm^{-1}. If we take the centers of the broad bands at ν = 381 and 402 cm^{-1}, respectively, as a measure of the band frequencies, then the small isotope frequency ratio of $\sim$1.055 and the broad band width indicate that it is due to a new Li-defect complex. It is also indicated that a significant part of the kinetic energy of the vibrational motion is not associated with the Li-species.

Natural Li-doped ZnSe (100 ppm) in which Li was introduced during crystal growth was also measured. It shows all of the ^{7}Li bands present in the Li-diffused samples except the one at $\nu = 420$ cm^{-1} which is too weak to distinguish from the strong two phonon band at $\nu = 421$ cm^{-1}. Lithium was also diffused into a CVD sample grown at Raytheon Corp. A lower diffusion temperature (600°C) and a longer time (24 hours) was used to avoid damaging the highly polycrystalline sample. The result was very similar to that discussed above for the grown material which was diffused at 700°C for four hours.

Lithium isotope mixtures were used as the diffusion source in an attempt to determine if any of the Li modes were coupled vibrations involving the motion of two or more Li atoms. No new LVM bands were observed. This indicates that all the localized vibration modes which are observed likely originate from defects involving only one Li atom/defect. This result is completely different from that for Li-diffused, undoped GaAs, where lithium forms at least five different types of defect complexes. All of these complexes contain more than one Li atom and the LVM are all strongly coupled vibrations. We therefore conclude that:

(1) Li diffused ZnSe (undoped) has 6 bands related to Li defects and all bands show an isotopic shift indicating that the vibrational energy resides almost totally in the Li atoms.

(2) Mixed Li isotopic doping gives no new bands indicating either one Li/defect or almost no coupling if there is more than one Li/defect.

(3) Li diffusions at different temperatures and for different times indicate that one of the bands is not from the same defect(s) as the other five bands.

(4) None of the bands observed here are the same as those reported by Mitsuishi et al. Moreover we have never observed the previous reported bands in any of the samples measured in this study.

From these results one can speculate concerning the nature of the Li defects as follows:

(a) Since the 350(375) cm^{-1} band appears to be unrelated to any others it must arise from a Li defect with a symmetry which is not lower than tetrahedral. One possible defect would be Li_{Zn} which is expected to be an acceptor with an ionization energy of $E_A \sim 0.114$ eV. If this is the case then for the prolonged and high temperature anneals in which the 350(373) cm^{-1} band increases dramatically, a similar increase in donor concentration would be required. There is however no independent evidence which supports this possibility. Moreover, experiments involving ZnSi:Al + Li would indicate the frequency of Li_{Zn} is considerably larger than 350(375) cm^{-1}.

(b) The remaining five bands, which show a nearly full Li isotope shift, require either a defect with two weakly coupled Li atoms per defect with the Li atoms in inequivalent sites or at least two differect types of defects with one or more Li atoms per defect for each.

C. Li diffused n-type ZnSe (Al, Ga)

It is believed that Al(Ga) is a substitutional, shallow state, effective mass donor when present in the form of Al_{Zn}. However, the fact that the samples in the as-grown state are highly compensated, the analysis of past photoluminescence studies, and the observation of six Al-related LVM bands in ZnSe:Al all tend to indicate that Al participates in one or more defect complexes. The previous LVM measurements[7] of ZnSe:Al and ZnSe:Al counterdoped with Cu, Ag, and Au indicated that one band, located at $\nu = 359\ cm^{-1}$, had a different behavior than the remaining bands, and it was attributed to the Al_{Zn} defect. The remaining bands are related to a complex(s) involving Al. The annealing study[6] under controlled Se pressure discussed in part III-a is in agreement with this identification of the $359\ cm^{-1}$ band, but this study as well as the previous ones leaves the five remaining Al-related bands in ZnSe:Al essentially unexplained.

There has been a previous study by Ibuki et al.[9] of ZnSe:Al + Li. This study was largely prompted by earlier successes in using Li as a compensating species in GaAs which was doped with a variety of impurities. The Li compensates the crystals by forming complexes, and the Li-related LVM helped identify and characterize the defect complexes. It is known from photoluminescence studies of ZnSe that Li_{Zn} is a shallow acceptor and pairs with donors such as Al and Ga as $Al(Ga)_{Zn}-Li_{Zn}$. In the Ibuki et al. study the Li and Al were introduced during ZnSe crystal growth, and the spectra obtained depended upon the doping concentrations. In their attempts to assign bands to vibrational modes of proposed defect centers they were forced to make some assumptions without adequate justification. However as will be shown, most of their assumptions were correct. For example, when the Li concentration << Al concentration, a new band at 412(383) cm^{-1} for $^6Li(^7Li)$ was assigned to an unassociated Li acceptor, presumeably Li_{Zn}. When the Li concentration ≈ Al concentration a band at exactly the same frequency was assigned to one of the Li modes of a Al_{Zn}-Li_{Zn} pair. Moreover, the strength of the 383 cm^{-1} relative to the other bands of the pair was different from that for the 412 cm^{-1} in the high Li concentration case making the isotopic identification questionable. The same type of situation existed for the 359 cm^{-1} band which at high Li concentration became assigned to an Al vibration of Al_{Zn}-Li_{Zn} pairs rather than the triply degenerate vibration of isolated Al_{Zn} donors.

The above results indicated that a further study of ZnSe:Al + Li is desireable. We have made a number of measurements for this system and for ZnSe:Ga + Li as well. Illustrative spectra for each of these cases are shown in Fig. 3 at the end of this section. The samples were Li-diffused ZnSe doped with 300 ppm of Al or an unknown concentration of Ga.* The experimental results and qualitative conclusions can be summarized as follows:

(1) ZnSe:Al samples which were annealed under different Se pressures (see part III-A of this report) prior to Li diffusion showed bands after Li diffusion which were reduced in the same manner as the 5 Al bands (not the Al_{Zn} at 359 cm^{-1}) in the pre-diffused sample. This includes the post-diffusion 359 cm^{-1} band thus indicating that this band may indeed be due to

---

*The figure from the supplier was 3000 ppm however the intensity of the observed LVM spectra would seem to indicate a much lower concentration.

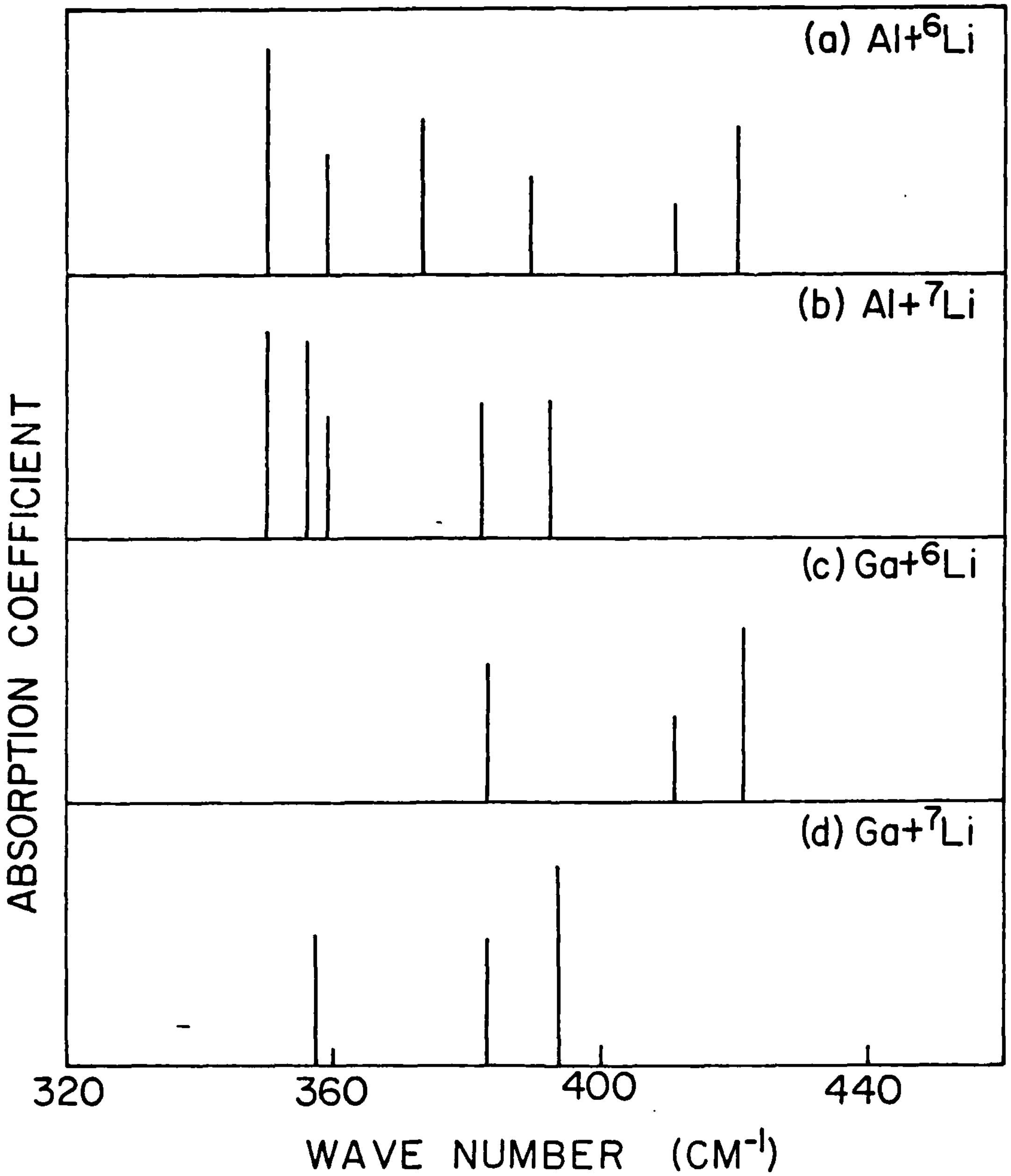
(a) Al+^{6}Li
(b) Al+^{7}Li
(c) Ga+^{6}Li
(d) Ga+^{7}Li
ABSORPTION COEFFICIENT
320
360
400
440
WAVE NUMBER (CM^{-1})

FIG. 3

different defects in ZnSe:Al and ZnSe:Al + Li.

(2) The 359 and 350 cm^{-1} bands which appear in both ZnSe:Al-^{7}Li(^{6}Li) samples do not appear in either ZnSe:Ga-^{7}Li(^{6}Li) and thus these bands are attributed to Al modes of the Al_{Zn}-Li_{Zn} pair. This conclusion is in agreement with Ibuki et al.

(3) Six bands are observed in the Al + ^{6}Li samples and only five in Al + ^{7}Li samples. With the exception of the 359 cm^{-1} discussed above all of the bands differ in frequency from those in the Al-doped samples. Here, as in the Ibuki work, the 383 cm^{-1} band of the Al + ^{7}Li spectrum was much larger than expected by its isotopic counterpart at 412 cm^{-1} in Al + ^{6}Li samples. This suggests the reason that only five bands are observed in the Al + ^{7}Li spectrum is due to the 383 cm^{-1} absorption band is the result of the superposition of two bands, one of which is the 412 cm^{-1} band in the ^{6}Li diffused samples.

(4) In comparing the Al + ^{6}Li and Al + ^{7}Li spectra, two bands show no shift (350 cm^{-1} and 359 cm^{-1}) and two show almost a full Li isotopic shift (420 cm^{-1} → 392 cm^{-1} and 412 cm^{-1} → 383 cm^{-1}). The remaining two bands show substantially less than the full isotopic shift (389 cm^{-1}, 373 cm^{-1} → 383 cm^{-1}, 356 cm^{-1}) indicating compled modes involving both Al and Li vibrational motion. This result suggests the Al_{Zn}-Li_{Zn} type of defect proposed in photoluminescence studies and a model based on this defect is applied to both the Al_{Zn}-Li_{Zn} and Ga_{Zn}-Li_{Zn} observations in part IV of this report.

D. Hardness of ZnSe; Annealing Effect

As mentioned previously the samples purchased from Eagle-Picher Corp. are polycrystalline with large size grains. The grain size, which is approximately $10^{-3} \geq$ volume $\geq 10\ mm^3$, depends somewhat upon the dopant concentration. Indentations were made on the central area of each grain in order to minimize grain boundary effects. Measurements were made with undoped and doped samples to determine if there is an impurity effect.

1. Undoped ZnSe

The procedure employed is first to make at least five groups of approximately five indentations each aligned parallel in an arbitrary direction, then rotate the sample 90° and make another similar five groups of indentations. The average of more than twenty readings in one direction was computed. The result based on five different large size grains from two ingots indicates that within the experimental accuracy the material is isotropic. The K.H.N. is 77.2 and the scatter of the readings is less than ± 4%. In regions close to the grain boundaries, the hardness is greater by about 15% ∿ 20%.

2. Al-doped ZnSe; 100 ppm and 300 ppm

For heavily Al-doped ZnSe, chemical polishing reveals some "parallel strips" on the surface. The origin of these strips is not known, and we have not had the opportunity to investigate them. Indentations were made along the directions perpendicular to (⊥) and parallel to (∥) the stripes. In all but one case, the K.H.N. (⊥) is smaller than the K.H.N. (∥). For the more heavily doped ZnSe:Al (300ppm), the difference in the K.H.N. between the two directions is about 10% while the scatter of the measurements for a given condition is generally with ± 4%. The K.H.N.

values are shown in Table 1. The results are compatible with previous measurements we made which used heavier loads, e.g. load $\geq$ 200 gm. The results indicate that ZnSe is hardened by the addition of Al and the K.H.N. increase can be by as much as 40% for ZnSe:Al with an Al concentration $\simeq$ 300 ppm.

3. Annealing effect ZnSe:Al (300 ppm)

Hardness measurements were made on the heat-treated samples to determine the effect of annealing on the microhardness. Usually the samples have some slight surface deterioration after annealing, and need repolishing. There is no measureable difference in the K.H.N. value before and after repolishing the samples surface. Results from three different ingots (with Al 300 ppm) are shown in Table 2. The microhardness in both directions decreases after annealing at 900°C in a Se partial pressure of 2 atms. After the first 40 hours of annealing, the K.H.N. values decrease about 10%, and the amount of decrease in the next 40 hours of annealing is less than 5%. There is a similarity between the observed decrease in the microhardness and the decrease in the band strength of five unknown Al-related bands. It indicates that there may be a simple relationship between the defects associated with five unknown Al-related bands and the defects associated with the change in the microhardness. There is however, insufficient data to establish a quantitative correlation. As previous mentioned the LVM spectra indicates the presence of a defect complex(s) involving Al but the specific complex(s) could not be identified with certainty. If the complex were known then we are also unaware of any theory relating the microhardness of semiconductors to the concentrations of specific types of defect species. Therefore only the

Table 1

	ZnSe(undoped)	ZnSe:Al(100ppm)	ZnSe:Al(300ppm)
K.H.N.(⊥)	77.2	86.9	103.5
K.H.N.(II)		92.3	113.6

Table 2.

Sample No. Sample condition	300-22		300-24		300-8
	K.H.N. ⊥	K.H.N. ∥	K.H.N. ⊥	K.H.N. ∥	K.H.N. average
before annealing	103.8	114.0	105.0	114.7	110.9
after 900°c/40hrs/Se-2atms	93.9	107.1	95.8	105.5	96.3
after 900°c/80 hrs/Se-2atms	92.2	102.2			92.5

following qualitative conclusions can be drawn;

1 The addition of Al hardens ZnSe

2 Annealing Al-doped ZnSe can reduce the microhardness

3 The reduction in microhardness in the annealing may be related to the changes in an Al-related defect complex(s) concentration.

IV. Model

In this section a simple valence-force type of model calculation will be given for the Al_{Zn}-Li_{Zn} and Ga_{Zn}-Li_{Zn} defects. First let us briefly review the experimental features to be fitted by the model. The Al + ^{6}Li doped ZnSe has 6 absorption bands and the Al + ^{7}Li has only 5 bands. Comparing the two spectra it appears that two modes do not change frequency at all, the two highest frequency modes for ^{6}Li show almost a "full Li isotopic shift" when ^{6}Li is replaced by ^{7}Li, and the remaining two modes show only a partial shift with one mode superimposing on one of the ^{7}Li modes. We therefore anticipate that two modes will be Al-like, two Li-like, and two will be coupled modes. If the Al is replaced by Ga in the model the larger Ga mass can be expected to greatly reduce the Al mode frequencies so that they merge with the band mode continuum and are no longer LVM. Thus one expects only three Li-like modes with frequencies which show almost a full isotopic shift.

The model used to estimate LVM frequencies for ZnSe:Al(or Ga) + Li employs the following assumptions:

a) The Al is a substitutional donor on a Zn site, Al_{Zn}, and Li acts a compensating acceptor Li_{Zn} a 2nd nearest neighbor site.

b) Since the masses of Li and Al are much less than those of Zn and Se, we treat both impurity atoms as vibrating against a rigid lattice.

c) The forces acting on the Al(Li) are between it and its four tetrahedrally arranged Se nearest neighbors plus the interaction between the Al and Li. For this simple model we neglect forces from more distant neighbors.

d) The interaction between the Al and Li is the sum of the attractive Coulomb force and a short range force. The force constant is treated as an experimentally determined factor, and

e) Lattice distortion is introduced by changing the bond angles between the Al(Li) and its four surrounding Se atoms. The distortion reduces the symmetry of the potential at the Al(Li) site and produces the frequency splitting. The small but non-zero isotope shift for two of the modes (see part III-C of this report) indicates that a strong coupling model with the changes in the equilibrium positions of the Al and Li should also be introduced.

Fig. 4 defines the coordinate system. The angles and atomic coordinates are also given in the figure. The black atom #1 at (0,0,0) represents the Al and #2 is the Li. The "a" is the lattice constant of ZnSe. The white atoms #3 → #9 represent the Se atoms which are the nearest neighbors to the impurities.

The equations of motion are

$$m_i \ddot{r}_{i\alpha} = \sum_{j,\beta} F^{ij}_{\alpha\beta} \; r_{j\beta}$$

or in matrix form

$$\mathbb{M} \cdot \ddot{\vec{r}} = \mathbb{F} \cdot \vec{r}$$

where i labels the atoms, "1" for the Al and "2" for the Li, and α labels the Cartesian coordinates. The m_i is the mass of the i th atom, $r_{i\alpha}$ is the α: component of the displacement from equilibrium of the i th atom. $F^{ij}_{\alpha\beta}$ represents the coupling constant between the α component of the displacement of the i th atom and the β component of the j th atom, and is defined as

$$F^{ij}_{\alpha\beta} = -\frac{1}{2} \frac{\partial^2}{\partial r_{i\alpha} \, \partial r_{j\beta}} \left[\phi(i,j) \right] ,$$

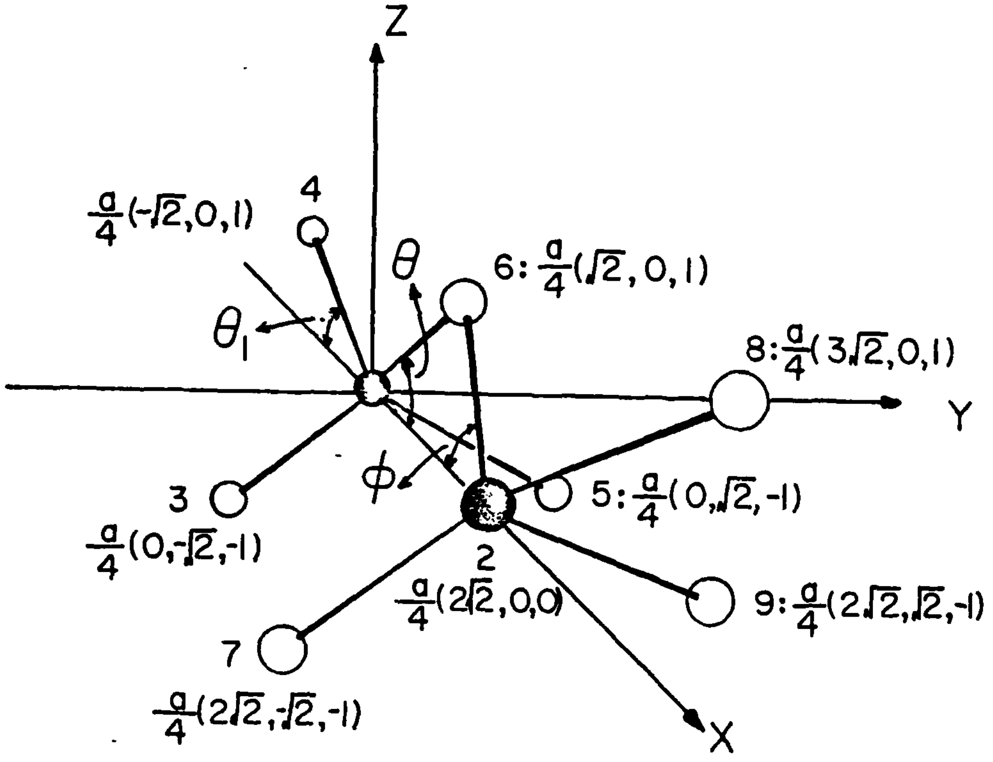
Z
4
$\frac{a}{4}(-\sqrt{2},0,1)$
θ
θ_1
6: $\frac{a}{4}(\sqrt{2},0,1)$
8: $\frac{a}{4}(3\sqrt{2},0,1)$
Y
ϕ
3
$\frac{a}{4}(0,-\sqrt{2},-1)$
5: $\frac{a}{4}(0,\sqrt{2},-1)$
2
$\frac{a}{4}(2\sqrt{2},0,0)$
9: $\frac{a}{4}(2\sqrt{2},\sqrt{2},-1)$
7
$\frac{a}{4}(2\sqrt{2},-\sqrt{2},-1)$
X

FIG. 4

where $\Phi(i,j)$ is the interaction potential between the particle i and j. $\mathbb{F}$ is a symmetrical 6 x 6 matrix which can be separated into four submatricies.

$$\left(F^{ij}_{\alpha\beta}\right) = \mathbb{F} = \left(\begin{array}{c|c} F^{11}_{\alpha\beta} & F^{12}_{\alpha\beta} \\ \hline F^{21}_{\alpha\beta} & F^{22}_{\alpha\beta} \end{array}\right)$$

where $(F^{11}_{\alpha\beta})$, $(F^{12}_{\alpha\beta})$, $(F^{21}_{\alpha\beta})$ and $(F^{22}_{\alpha\beta})$, are four 3 x 3 matricies.

The lower left hand submatrix $F^{21}_{\alpha\beta}$ is the transverse of the upper right hand quarter $F^{12}_{\alpha\beta}$. Both of them represent the coupling force matricies between particles 1 and 2. We assume that the interaction between Al and Li is the sum of the attractive Coulomb potential ϕ^c and a short range potential ϕ^s. Then the elements of the upper right hand quarter $F^{12}_{\alpha\beta}$ can be written as

$$F^{12}_{\alpha\beta} = -\frac{\partial^2}{\partial r_{1\alpha}\,\partial r_{2\beta}}\left(\phi^c + \phi^s\right)\Big|_{r=r_0} ,$$

Since both Φ^c and Φ^s are functions of the distance between particles 1 and 2, r_{12} only, i.e. $\Phi^c = \Phi^c(r_{12})$ and $\Phi^s = \Phi^s(r_{12})$. Then we can calculate the derivatives

$$\frac{\partial^2\phi^c}{\partial x_1\,\partial x_2} = -\frac{2\,\theta_1\,\theta_2}{\epsilon\, r_{12}^3} ,$$

$$\frac{\partial^2\phi^c}{\partial y_1\,\partial y_2} = \frac{\partial^2\phi^c}{\partial z_1\,\partial z_2} = \frac{\theta_1\,\theta_2}{\epsilon\, r_{12}^3} ,$$

$$\frac{\partial^2\phi^s}{\partial x_1\,\partial x_2} = \frac{\partial^2\phi^s(r_{12})}{\partial r_{12}^2} = -\phi^{s\,\prime\prime} ,$$

$$\frac{\partial^2\phi^s}{\partial y_1\,\partial y_2} = \frac{\partial^2\phi^s}{\partial z_1\,\partial z_2} = \frac{\partial\phi^s(r_{12})}{r_{12}\cdot\partial r_{12}} = -\frac{1}{r_{12}}\,\phi^{s\,\prime} ,$$

and

$$\frac{\partial^2\phi^c}{\partial X_1\,\partial Y_2} = \frac{\partial^2\phi^c}{\partial X_1\,\partial Z_2} = \frac{\partial^2\phi^s}{\partial X_1\,\partial Y_2} = \frac{\partial^2\phi^s}{\partial X_1\,\partial Z_2} = 0$$

Where Q_1 and Q_2 = the "effective charge" of the Al and Li, ϵ = the relative dielectric constant, r_o = the equilibrium distance between the Al and Li, $\phi^{s''}$ and $\phi^{s'}$ = the second and first derivatives of ϕ^s with respect to the interatomic distance γ_{12}. We can see that only the diagonal terms are not equal to zero. So

$$(F^{12}_{\alpha\beta}) = \begin{pmatrix} \frac{2Q_1Q_2}{\epsilon r_0^3} + \phi_s'' & 0 & 0 \\ 0 & -\frac{Q_1Q_2}{\epsilon r_0^3} + \phi_s' & 0 \\ 0 & 0 & -\frac{Q_1Q_2}{\epsilon r_0^3} + \phi_s' \end{pmatrix}$$

$$= \begin{pmatrix} \gamma & 0 & 0 \\ 0 & \delta & 0 \\ 0 & 0 & \delta \end{pmatrix}$$

The F^{12}_{xx}, F^{12}_{yy}, and F^{12}_{zz} will be determined by experiment.

The upper left quarter $F_{\alpha\beta}^{11}$ which represents the restoring force matrix can be split into the sum of Al-Se forces and Al-Li force,

$F_{\alpha\beta}^{11} = (F_{\alpha\beta}^{11})_{Al-Se} + (F_{\alpha\beta}^{11})_{Al-Li},$

where $(F_{\alpha\beta}^{11})_{Al-Li} = -(F_{\alpha\beta}^{12})$. We assume that Al-Se forces are hamonic forces with force constant K_1, then

$$(F_{\alpha\beta}^{11})_{Al-Se} = - \sum_{j=3,4,5,6} \frac{\partial^2}{\partial r_{1\alpha}\, \partial r_{j\beta}} \left(\frac{1}{2} K_1 r_{1j}^2 \right),$$

where r_{ij} = the interatomic distance between particles 1 and j and the summation is over four surrounding Se atoms. For example, the derivative $F_{x\beta}^{11}$ can be calculated, and then we get

$$(F_{xx}^{11})_{Al-Se} = -K_1 \cos^2\theta - K_1 \cos^2\theta_1 ,$$

$$(F_{xY}^{11})_{Al-Se} = 0 ,$$

and

$$(F_{xz}^{11})_{Al-Se} = - K_1 \cos\theta \sin\theta - K_1 \sin\theta_1 \cos\theta_1$$

The equation of motion of particle 1 in the x direction is then

$$m_1 \ddot{X}_1 = \sum_{\substack{j=1,2 \\ \beta=x,Y,Z}} F_{x\beta}^{1j}\, r_{j\beta}$$

$$= - \left[K_1 (\cos^2\theta + \cos^2\theta_1) + \Phi_s'' + \frac{2\theta_1 \theta_2}{\epsilon r_0^3} \right] X_1$$

$$- \left[K_1 \cos\theta \sin\theta + K_1 \cos\theta_1 \sin\theta_1 \right] Z_1 + \left(\frac{2\theta_1\theta_2}{\epsilon r_0^3} + \Phi_s'' \right) X_2$$

$$+ \left(-\frac{\theta_1\theta_2}{\epsilon r_0^3} + \frac{1}{r_0} \Phi_s' \right) Z_2$$

Lattice distortion is introduced by letting the Al-Se and Li-Se bonds change in length and angle. The strong Al-Li coupling can push both Al and Li off their Td symmetry site and alter the Al-Se and Li-Se bonds. For simplicity, we assume that the change only occurs in the Al-Se(#6) and Li-Se(#6) bonds. The elements of the force constant can be written as follows:

$$F^{11}_{XX} = -\frac{4}{3}K_1 - (K_1 + \Delta K_1)(\cos^2\theta - \frac{2}{3}) - \frac{2}{3}\Delta K_1 - \gamma \tag{4.1}$$

$$F^{11}_{XY} = F^{11}_{YX} = F^{11}_{YZ} = F^{11}_{ZY} = 0 \tag{4.2}$$

$$F^{11}_{YY} = -\frac{4}{3}K_1 - \delta \tag{4.3}$$

$$F^{11}_{XZ} = -(K_1 + \Delta K_1)\sin\theta\cos\theta + K_1 \cdot \frac{\sqrt{2}}{3} \tag{4.4}$$

$$F^{11}_{ZZ} = -\frac{4}{3}K_1 - (K_1 + \Delta K_1)(\cos^2\theta - \frac{2}{3}) - \frac{1}{3}\Delta K_1 - \delta \tag{4.5}$$

$$F^{12}_{XX} = \gamma \tag{4.6}$$

$$F^{12}_{YY} = F^{12}_{ZZ} = \delta \tag{4.7}$$

$$F^{12}_{\alpha\beta} = 0 \quad \text{if } \alpha \neq \beta \tag{4.8}$$

$$F^{21}_{\alpha\beta} = F^{12}_{\beta\alpha} \tag{4.9}$$

$$F^{22}_{XX} = -\frac{4}{3}K_2 - (K_2 + \Delta K_2)(\cos^2\phi - \frac{2}{3}) - \frac{2}{3}\Delta K_2 - \gamma \tag{4.10}$$

$$F^{22}_{XY} = F^{22}_{YX} = F^{22}_{ZY} = F^{22}_{YZ} = 0 \tag{4.11}$$

$$F^{22}_{YY} = -\frac{4}{3}K_2 - \delta \tag{4.12}$$

$$F^{22}_{XZ} = (K_2 + \Delta K_2)\sin\phi\cos\phi - K_2 \cdot \frac{\sqrt{2}}{3} \tag{4.13}$$

$$F^{22}_{ZZ} = -\frac{4}{3}K_2 + (K_2 + \Delta K_2)(\cos^2\phi - \frac{2}{3}) - \frac{1}{3}\Delta K_2 - \gamma \tag{4.14}$$

where K_1 = the force constant of the Al-Se bond

ΔK_1 = the change in the force constant of the Al-Se bond

K_2 = the force constant of the Li-Se bond

ΔK_2 = the change in the force constant of the Li-Se bond

Because the Cs symmetry, the vibrations perpendicular to the mirror plane are uncoupled from the vibrations in the plane. The eigenfrequencies cies and eigenvectors are obtained by diagonalizing a 2 x 2 matrix B^1 and a 4 x 4 matrix B^2, respectively, where

$$B^{ij}_{\alpha\beta} = - F^{ij}_{\alpha\beta}/(m_i m_j)^{1/2} ,$$

$$B^1 = \begin{pmatrix} B^{11}_{YY} & B^{12}_{YY} \\ B^{21}_{YY} & B^{22}_{YY} \end{pmatrix}$$

and

$$B^2 = \begin{pmatrix} B^{11}_{xx} & B^{11}_{xz} & B^{12}_{xx} & B^{12}_{xz} \\ B^{11}_{zx} & B^{11}_{zz} & B^{12}_{zx} & B^{12}_{zz} \\ B^{21}_{xx} & B^{21}_{xz} & B^{22}_{xx} & B^{22}_{xz} \\ B^{21}_{zx} & B^{21}_{zz} & B^{22}_{zx} & B^{22}_{zz} \end{pmatrix}$$

If we assume that when there is no Al-Li coupling and no lattice distortion, then the two triply degenerate eigenfrequencies are the local mode frequencies of Al_{Zn} and Li_{Zn}, respectively, which then yield K_1 and K_2 as experimentally determinded parameters. With no Al-Li coupling the LVM frequencies are taken to be 359 cm^{-1} for Al_{Zn} (T_d symmetry) and 411 cm^{-1} for $^6Li_{Zn}$ ($T_d$symmetry). These choices for the uncoupled frequencies were discussed in earlier sections of this report.

When the Al-Li coupling is introduced the calculation proceeded as follows:

From equations 4-3 and 4-12 we note that the simple lattice distortion did not alter the force constants of Al_y and Li_y, where A_α denotes the α component of A vibration. If we further assume $\delta = 0$, then the Al_y and Li_y are decoupled from each other and would have the same frequencies as $\nu(Al_{Zn})$ and $\nu(Li_{Zn})$, respectively. The 359 cm^{-1} band is thus assigned to the local model of Al_y and the 411 (or 383) cm^{-1} band to the local mode of Li_y.

The 4 x 4 matrix B^2 is diagonalized to get the eigenfrequencies and eigenvectors of the coupled modes in the mirror plane. The local mode frequencies were computed as a function the x component of the Al-Li coupling constant γ in fig. 5. The paramenters θ, Φ, ΔK_1 and ΔK_2 are chosen so that when $\gamma = 0$, the frequencies follow the order, $\nu(Li_z) > \nu(Li_x) > \nu(Al_x) > \nu(Al_z)$. Because with $\delta \neq 0$ and $\delta = 0$ the Al-Li coupling is only in the x direction, modes 1 and 4 remain essentially Li_z-like and Al_z-like, respectively. Their eigenfrequencies decrease slightly as γ increases while those for modes 2 and 3 decrease rapidly. When the coupling is weak, ν (mode 2) decreases faster than ν (mode 3) because the former consists primarily of Li_x vibration and the latter primarily of Al_x vibration. But as the coupling increases and ν (mode 2) approaches ν (mode 3) the two modes become strongly mixed and there is no cross-over of the frequencies. When the coupling is weak the character of the mode 2 and 3 is that mode 2 is Li_x-like and the mode 3 is Al_x-like. For sufficiently strong coupling (γ large) they reverse character. Figure 6 shows the kinetic energy composition of the coupled modes 2 and 3, i.e. $\frac{KE(Li)}{KE(total)}$, as a function of the Al-Li coupling constant γ. If we replace the mass of Al by Ga while keeping the other parameters unchanged, then we will get the coupled modes for the Ga-Li pair. Because of the larger mass of Ga, the lower two modes which consist primarily of Ga vibration merge in the fundamental absorption band and do not appear in Fig. 5. The dashed line in the same figure shows the higher two modes 1' and 2' which consist primarily of Li vibration. Because the large energy difference between the Li_x and Ga_x vibration, mode 2' remains Li_x-like throughout the γ range in this figure.

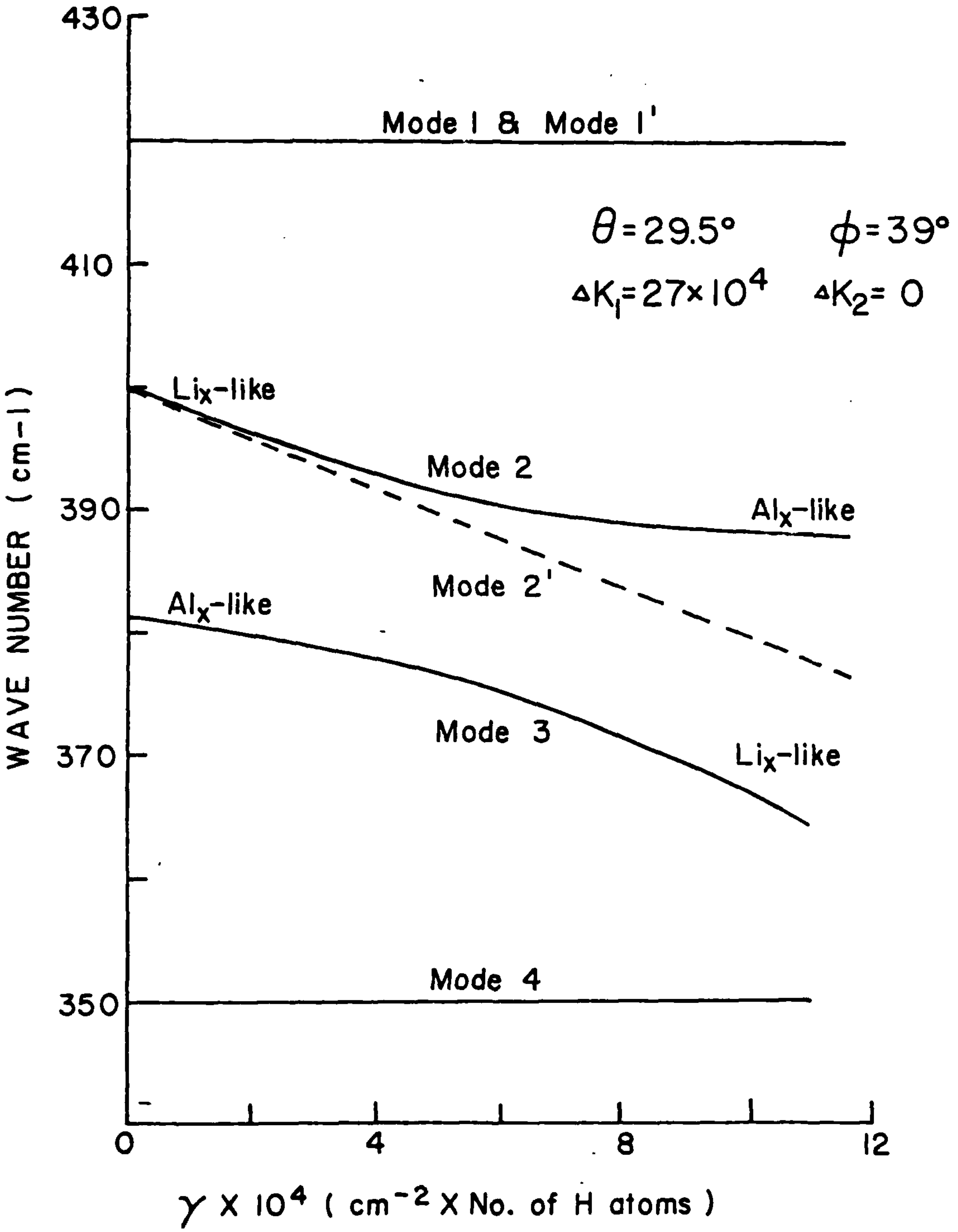

430
410
390
370
350
WAVE NUMBER (cm-1)
Mode 1 & Mode 1'
θ=29.5°
ϕ=39°
ΔK_1=27×10^4
ΔK_2= 0
Li$_x$-like
Mode 2
Al$_x$-like
Mode 2'
Al$_x$-like
Mode 3
Li$_x$-like
Mode 4
0
4
8
12
γ X 10^4 (cm^{-2} X No. of H atoms)

Fig. 5

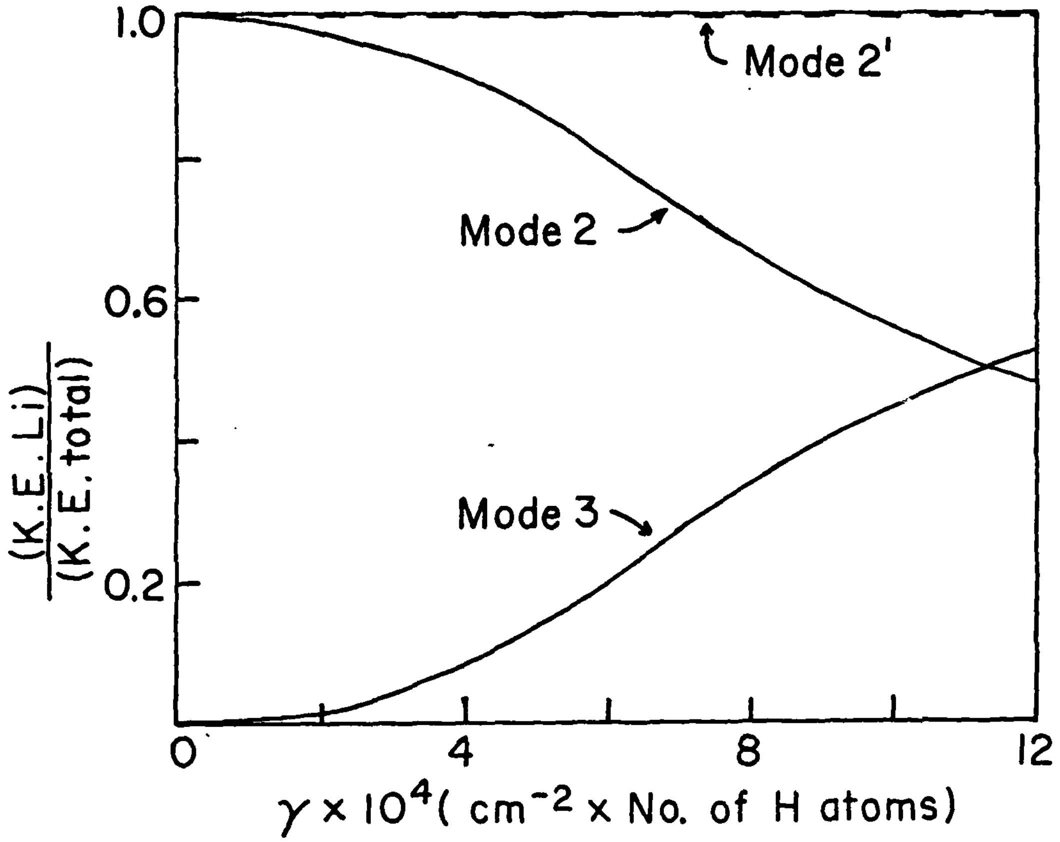
1.0
0.6
0.2
(K.E. Li) / (K.E. total)
0
4
8
12
$\gamma \times 10^4$(cm^{-2} x No. of H atoms)
Mode 2'
Mode 2
Mode 3

FIG. 6

We can estimate the Al-Li interaction from Fig. 5. The parameters for the best fitting of experimental data are given in Table 3. The amount of the lattice distortion in the Li site is less than the Al site. This is compatible with the fact that the tetrahedral covalent radius of Al is 1.26 Å and the ionic radius of Li is 2.26 Å. Thus the attractive Coulomb interaction between the Al and the Li could procude a new Al equilibrium position which is further from the original T_d site than that for the Li.

In the Al-^{7}Li system, we only replace the mass of ^{6}Li by ^{7}Li while keeping all the parameters unchanged. The frequency of mode 2"(^7Li_x-like) is smaller than that of the mode 3" (Al_x-like) even when the Al-Li interaction γ is zero as shown in Fig. 7. As we increase the interaction, the frequency of mode 2" decrease with a faster rate than the mode 3". Again the model frequencies do not cross-over, however in this case when there is strong Al-Li coupling, mode 3" remains Al_x-like and the mode 2" is Li_x-like. Figure 8 shows the kinetic energy composition of the coupled mode 2" and 3", i.e. $\frac{KE(Li)}{KE(total)}$, as a function of the Al-Li coupling constant γ. If γ becomes sufficiently large, there will be a cross-over region for the modes 2" and 4" (Al_z-like). The mode 2" will change from Li_x-like to Al_z-like and mode 4" will go from Al_z-like to Li_x-like.

This simple model explains that the 389 and 373 cm^{-1} bands in ZeSe:Al + ^{6}Li are the strong coupling modes while their corresponding 383 and 356 cm^{-1} bands in ZeSe:Al + ^{7}Li remain as Al_x-like and Li_x-like modes, respectively.

Table 3.

Geometric assumption	θ	ΔK_1	ϕ	ΔK_2	$\frac{Q_{Al} \cdot Q_{Li}}{\epsilon r_0^3}$ $\left(\begin{matrix}cm^{-2} \times \text{No.} \\ \text{of H atoms}\end{matrix}\right)^{\dagger}$
No lattice distortion	35.3	0	35.3	0	
Evaluation of Coulomb term in Al-Li interaction where $Q_{Al} = Q_{Li} = e$ and $\epsilon = 5$					5.5×10^5
Al-^{6}Li & Al-^{7}Li	29.5°	2.7×10^5	39°	0	6.5×10^4
Ga-^{6}Li & Ga-^{7}Li	29.5°	2.7×10^5	39°	0	6.5×10^4

FIG.7

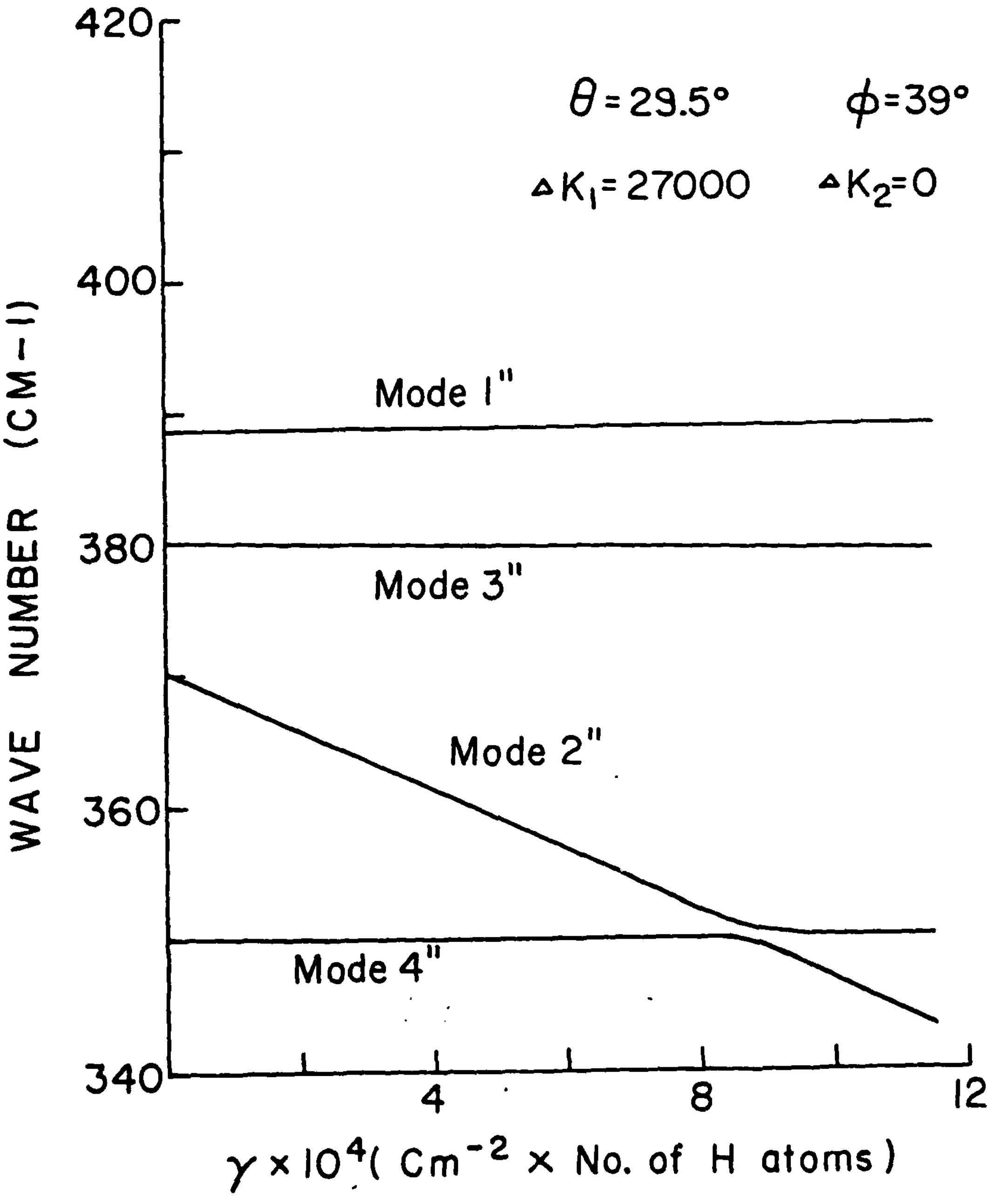

$\theta = 29.5°$
$\phi = 39°$
$\Delta K_1 = 27000$
$\Delta K_2 = 0$
Mode 1"
Mode 3"
Mode 2"
Mode 4"
420
400
380
360
340
4
8
12
WAVE NUMBER (CM-1)
$\gamma \times 10^4$ (Cm^{-2} × No. of H atoms)

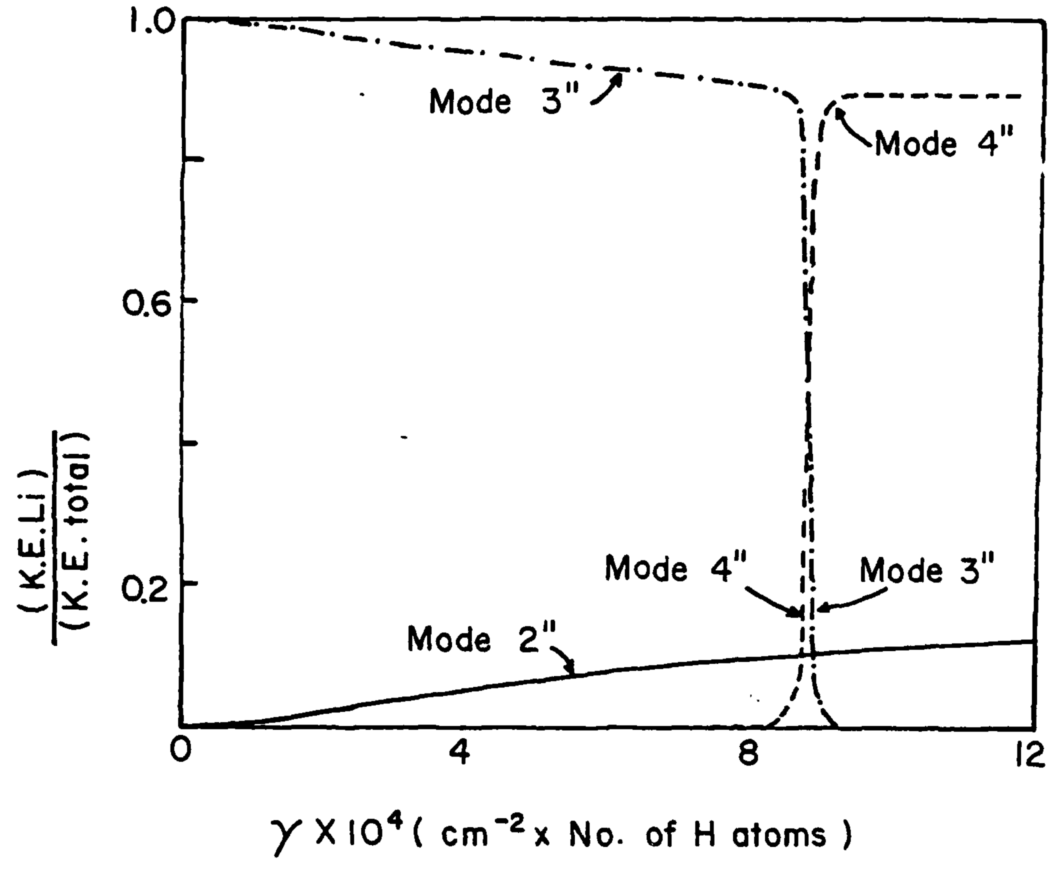
1.0
0.6
0.2
0
4
8
12
(K.E.Li) / (K.E. total)
γ X 10⁴ (cm⁻² x No. of H atoms)
Mode 3"
Mode 4"
Mode 4"
Mode 3"
Mode 2"

FIG. 8

References

1. R. C. Newman, Infrared Studies of Crystal Defects (Barnes and Noble, New York, 1973)
2. M. E. Levy and W. G. Spitzer, J. Phys. C: Solid State Phys. 6 3223 (1973)
3. V. Swaminathan and S. M. Copley, J. Appl. Phys. 47, 4405 (1976).
4. The segregation coefficient of Al or Ga in ZnSe is not known and because there is some uncertainty as to whether the growth was done near equilibrium conditions, we do not know the impurity concentration in the crystal. The concentrations specify the dopant added to the charge from which the ingot was grown.
5. J. L. Merz, K. Nassau and J. W. Shiever, Phys. Rev. B8, 1444 (1973).
6. A. Mitsuishi, A. Manabe, H. Yoshinaga, S. Ibuki and H. Komiya Prof. Theor. Phys. Supp. 45, 21 (1970).
7. B. V. Dutt and W. G. Spitzer, J. Appl. Phys. 47, 573 (1976).
8. A. Mitsuishi, A. Manabe, Proc. Intern. Conf. Phys. Semicond. (Kyoto) 72 (1966).
9. S. Ibuki, H. Komiya, A. Mitsuishi, A. Manabe, and H. Yoshinaga, Proceedings of the IX International Conference on II-VI Semiconducting Compoun s, edited by D. G. Thomas (Benjamin, New York, 1967), p. 1140.

FILMED

9-8